1969

Investigations of some rhenium compounds and the structure of the mesoperrhenate ion

William Andrew Gault
Iowa State University

INVESTIGATIONS OF SOME RHENIUM COMPOUNDS AND THE STRUCTURE OF THE MESOPERRHENATE ION

by

William Andrew Gault

A Dissertation Submitted to the
Graduate Faculty in Partial Fulfillment of
The Requirements for the Degree of
DOCTOR OF PHILOSOPHY

Major Subject: Physical Chemistry

Approved:

Signature was redacted for privacy.

In Charge of Major Work

Signature was redacted for privacy.

Head of Major Department

Signature was redacted for privacy.

Dean of Graduate College

Iowa State University
Ames, Iowa

1969

TABLE OF CONTENTS

TABLE OF CONTENTS (Continued)

INTRODUCTION

Rhenium is one of the rarest elements in the earth's crust with an estimated average concentration of 0.001 ppm (1). Rhenium has not been identified in nature as a major constituent of a mineral, but often it occurs in trace amounts in a number of different minerals. The composition of minerals or mineral concentrates is usually considered high in rhenium when it exceeds 10 ppm. Certain molybdenite concentrates, recovered as a by-product of copper mining, are known to contain rhenium in concentrations between 100 and 3000 ppm. These concentrates are the major commercial source of rhenium. During the usual processing of the concentrates, a roasting step produces molybdic oxide and also converts rhenium into oxides which may be collected as flue dust or scrubbed from flue gases. The molybdic oxide produced from these concentrates is given the primary economic consideration during roasting, and the rhenium may be recovered as a by-product. Although the processing of rhenium-bearing molybdenite has a direct relationship to the availability of rhenium, the production of rhenium depends mostly on the willingness of processors to recover it and the efficiency of the methods employed. Furthermore, since most of the rhenium is released

into flue gases, failure to recover rhenium at this point results in a permanent loss. The existing rhenium supply appears adequate to meet near-term needs, however, a long-term shortage could develop unless rhenium resources are managed more effectively. Estimates of the amount of rhenium released annually from domestic molybdenite roasting range from 12,000 to 28,000 pounds (2), yet in 1962 only 1000 pounds of rhenium were produced (3). Even though production improved to 8000 pounds by 1967 (3), it appears that large quantities of rhenium were still being wasted, and the cost of rhenium still remains high. A more effective handling of rhenium resources would probably result if stable markets were developed and better rhenium recovery methods were devised or certain existing methods improved.

In spite of its high price, rhenium exhibits certain unique properties that make it attractive for specialized physical and chemical applications. A high melting point, high electrical resistivity, high temperature mechanical strength, and favorable thermoelectric properties qualify rhenium metal as a promising high temperature material. Weldability and ductility over a wide temperature range make rhenium and some of its alloys attractive for the fabrication

of shapes for special purposes. Finely divided rhenium metal, some rhenium oxides, and some rhenium sulfides behave as catalysts in certain organic and inorganic reactions. Rhenium metal shows high corrosion resistance to sulfuric and hydrochloric acids, and rhenium is not attacked by molten tin, zinc, silver, or copper. Although these properties of rhenium are attractive for commercial applications, the high cost of rhenium will probably limit usage to very specialized areas where the performance of rhenium or rhenium compounds would be economically favorable. The demand for rhenium, therefore, will depend largely on the development of specific uses which justify the high cost. Although much is already known about rhenium, there is still need for research on rhenium chemistry and metallurgy in order to obtain more knowledge of rhenium materials and develop new processing techniques and new uses.

The research described in this presentation can be divided into two broad areas: one directed toward improving the collection of rhenium from rhenium-bearing molybdenite concentrates, and the other pertaining to basic rhenium chemistry. If an economical method could be developed for direct extraction of rhenium from molybdenite concentrates, rhenium could be collected without regard to certain molybdenum considera-

tions. However, if direct extraction would not be feasible, further basic knowledge about the rhenium oxides and the interrelationship of these oxides might be applied to improve the recovery of rhenium, especially from roaster flue gases. Studies related to the direct extraction of rhenium from molybdenite concentrates and investigations of some rhenium oxides are part of the research described here.

Chemically related to the yellow rhenium oxide, Re_2O_7, is a mesoperrhenate ion. Some properties of mesoperrhenate salts have been known since the 1930's, but detailed studies of the mesoperrhenate ion are lacking. Therefore, the identity and geometrical structure of this ion were studied, and the results are reported here.

BACKGROUND

Discovery of Rhenium

In 1871 D. I. Mendele'eff proposed the Periodic Law of the Chemical Elements which related the periodicity of the elements to their atomic weights (4). Mendele'eff arranged the known elements in a periodic table designating blank positions and assigning provisional names to then undiscovered elements. To the unknown element in the same family as manganese and positioned between tungsten and osmium he assigned the name tri-manganese, later changing it to dvi-manganese in 1905 (5). By 1909 the discovery of dvi-manganese had been claimed by several workers, but these claims were either disproved or generally considered unfounded (6). In 1913 Moseley showed a relationship between the characteristic X-ray spectrum of an element and the atomic number of that element. This discovery led to a new form of the periodic law relating the periodicity of the elements to their atomic numbers, instead of their atomic weights. In the new periodic table dvi-manganese still remained between tungsten and osmium and was assigned atomic number 75.

The discovery of dvi-manganese in 1925 was the result of skillfully planned experiments carried out by the German

chemists W. Noddack, I. Tacke, and O. Berg (7). These investigators noted the failure of other workers to isolate dvi-manganese, and by comparison of the distributions and abundances of various neighboring elements, they concluded that dvi-manganese must be widely distributed in nature and exceedingly rare. If this were true, it would be almost impossible to detect naturally occurring dvi-manganese by characteristic X-ray emission, unless a preliminary enrichment was performed. On the basis of further chemical and geological considerations, some chemical properties of dvi-manganese were predicted, potential mineral sources were proposed, enrichment factors were estimated, and chemical schemes for enrichment were set forth. Initial studies were performed on platinum ores, but only limited quantities were available to the investigators, so the search was extended to other ores such as columbite, which contains small amounts of tungsten and osmium. Beginning with 1 kg of columbite, Noddack, Tacke and Berg extracted 20 mg of a concentrate. An X-ray spectrum of the concentrate was recorded and compared to the calculated L series for element number 75. As hypothesized, the concentrate contained dvi-manganese and the chemists called it "rhenium" in honor of the German Rhine. Further investiga-

tions by Noddack and Noddack[1] revealed that certain molybdenites contain a relatively high amount of rhenium, and in 1929 the Noddacks processed 660 kg of Norwegian molybdenite to recover the first one-gram quantity of rhenium metal (8).

Occurrence and Primary Sources of Rhenium

The Noddacks analyzed over 1800 minerals and found small amounts of rhenium in a variety of mineral types. A listing of some rhenium analyses made on certain minerals by the Noddacks and other investigators is presented in Table 1 along with the mineral names, geographical origins, and major constituents. Even though rhenium and manganese belong to the same subgroup of the periodic table, the rhenium analyses for pyrolusite, rhodonite, columbite, tantalite and wolframite indicate that rhenium concentrations in manganese-bearing minerals are relatively low. It is apparent from Table 1, however, that primary molybdenite concentrates and by-product molybdenite concentrates are relatively rich in rhenium when compared to other recognized sources.

The association of rhenium with molybdenite apparently has some unexplained fundamental significance. The Noddacks

---

[1]Walter Noddack had married Ida Tacke in 1926.

Table 1. The rhenium concentration in certain minerals

Mineral	Origin	Major constituents	Rhenium content (ppm)	
Pyrolusite	Bohemia	MnO_2	0.00	(9)
Rhodonite	Sweden	$MnSiO_3$	0.00	(9)
Columbite	Norway	$(Fe,Mn)Nb_2O_6$	0.2	(9)
Tantalite	South Africa	$Mn(Ta,Nb)_2O_6$	0.03	(9)
Wolframite	Czechoslovakia	$(Fe,Mn)WO_4$	0.02	(9)
Uranite	Arizona	UO_2	0.3-3.0	(2)
Wulfenite	USA, Chile	$PbMoO_4$	~0.1-2.	(10)
Aluite	Norway	$(Zr,Hf)SiO_4$	0.6	(9)
Gadolinite	Norway	$(Fe,Be)_2Y_2Si_2O_{10}$	0.03	(9)
Thortveitite	Norway	$Y_2Si_2O_7$	0.6	(9)
Platinum ore	USSR	?	0.01	(9)
Iron pyrite	Norway	FeS_2	0.01	(9)
Copper pyrite	Mansfield, Ger.	Cu_2S-$CuFeS_2$	0.02	(9)
Primary molybdenite concentrates				
	Siberia	MoS_2	0.6	(9)
	Climax, Colo.	MoS_2	1.8	(9)
	Climax, Colo.	MoS_2	10.0	(2)
	Japan	MoS_2	10.0	(9)
By-product molybdenite concentrates				
	Montana	MoS_2	300.	(11)
	Utah	MoS_2	360.	(11)
	Chile	MoS_2	500.	(11)
	Arizona	MoS_2	1000-2000.	(11)
	Norway	MoS_2	3100.	(2)

specifically determined the molybdenum to rhenium ratio in a total of seventeen sulfide, oxide, and silicate minerals (9). They found a Mo:Re weight ratio of 10^3-10^5:1 for sulfide minerals and 10^2-10^3:1 for silicate and oxide minerals. More recently Churchwood and Rosenbaum (2) analyzed an unstated number of different rhenium-bearing minerals (oxides and sulfides) and concluded that molybdenum was always present in minerals that gave a positive test for rhenium. Recently some Russian investigators have also reported the association between rhenium and molybdenum (12,13). Unfortunately none of the authors speculate on the fundamental aspects of the rhenium-molybdenum association.

Although molybdenites vary widely in rhenium content, they are nevertheless the most important commercial sources of rhenium. The analyses of several molybdenite concentrates, as presented in Table 1, are divided into two different groupings: by-product molybdenite concentrates and primary molybdenite concentrates. By-product molybdenite concentrates are recovered from certain porphyry copper deposits where copper is the chief valuable mineral and molybdenum is considered a by-product. Typical copper ores often average about 0.03 to 0.05 percent MoS_2. During the processing of these ores, a

concentrate containing copper sulfides and molybdenite is usually recovered after separation from the gangue minerals by crushing, screening, and flotation processes. The molybdenite is then separated from the copper sulfides by selective flotation and upgraded to yield a final molybdenite concentrate of 80 percent or more MoS_2. These by-product molybdenite concentrates can generally contain about 300 ppm or more rhenium. Since rhenium is later recovered as a by-product of molybdenite roasting, the rhenium obtained in this manner is a by-product of a by-product of certain copper mining operations.

In the recovery of primary molybdenite concentrates the molybdenum is the chief valuable mineral. From a primary source ore, usually averaging about 0.4 percent MoS_2, a low grade concentrate is recovered after separation from the bulk extraneous rock. The low grade concentrate is upgraded by several stages of fine grinding and flotation to yield a final molybdenite concentrate of 80 percent or more MoS_2. The rhenium contained in primary molybdenite concentrates usually averages less than 15 ppm.

The difference in rhenium concentrations between primary and by-product molybdenite concentrates is due to the rhenium

to molybdenum ratio in the original mineral deposits and does not relate to the mineral processing methods. In both cases the rhenium content in the original ore is less than 1 ppm, however, the rhenium to molybdenum ratio is larger in the porphyry copper ores, and this causes a greater enrichment of rhenium in the by-product concentrates. At the present time the by-product molybdenites provide the major sources of rhenium, and the rhenium in primary molybdenite ores is usually not recovered. This is unfortunate since about two thirds of the annual domestic molybdenum production is derived from primary molybdenite ores (14).

Commercial Recovery of Rhenium

Although many rhenium recovery processes have been devised, only three have been important to the domestic supply of rhenium.

The Feit process

The first commercial recovery and production of rhenium was carried out by W. Feit in 1930 (15,16,17). The rhenium was recovered from copper deposits located near Mansfield, Germany. These deposits contained about two percent copper along with small amounts of other elements including rhenium

and molybdenum. During processing of the copper ore, a complex sulfide slime containing rhenium and numerous other elements was formed. The slime was weathered in air for several months and then leached with an aqueous ammonium sulfate solution. The leachings were concentrated by evaporation, and double sulfates of ammonium with calcium, copper, nickel, and zinc precipitated. The solid double sulfates were removed by filtration, ammonium sulfate was added to the filtrate, and the filtrate was partially evaporated to precipitate complex compounds of phosphorus, vanadium and molybdenum. The process of evaporation and precipitation was repeated until only ammonium sulfate precipitated, and a pale yellow liquor remained. The addition of potassium chloride precipitated sparingly soluble potassium perrhenate which was subsequently purified by repeated dissolutions and recrystallizations. Hydrogen reduction of the perrhenate at red heat gave a mixture of rhenium metal and potassium compounds. A purified rhenium metal powder resulted when potassium compounds were removed by aqueous leaching.

The Tennessee process (17)

The rhenium produced by Feit was supplied to the United States and other countries until the outbreak of World War II.

At this time investigators at the University of Tennessee were performing research on rhenium, and as their supply dwindled, they began experimenting to produce rhenium from domestic sources. In the 1940's,Melaven and Bacon developed and patented a process for the extraction of rhenium from molybdenite roaster flue dusts. The dusts processed at the University of Tennessee were collected by the Miami Copper Co. of Miami, Arizona during the roasting of by-product molybdenite concentrates. The dusts contained unaltered molybdenite, water soluble molybdenum and rhenium compounds, and minor amounts of other materials. The rhenium content in the roaster dusts usually varied from 3000 to 16,000 ppm.

In the process employed at the University of Tennessee, a flue dust was mixed with water and the resulting solution was filtered to separate the water soluble molybdenum and rhenium species from the insoluble residues. Finely ground potassium chloride was added to the filtrate, and a light brown precipitate containing 85 to 95 percent potassium perrhenate was collected. The crude potassium salt was dissolved in boiling water and the hot solution was filtered to remove insolubles. The filtrate was cooled to recrystallize potassium perrhenate, and the crystals were recovered by filtration.

After a total of five dissolutions and recrystallizations, potassium perrhenate of acceptable purity was obtained.

At the University of Tennessee the production of rhenium metal from purified potassium perrhenate involved a high-pressure hydrogen reduction. A silver lined high-pressure reaction vessel was charged at room temperature with potassium perrhenate and hydrogen gas at 1000 to 1500 psi. The temperature of the vessel was raised to 235°C where a sudden drop in pressure indicated a reaction had started. Additional hydrogen was added to provide an excess of reductant, and the temperature was gradually raised to 350°C. After maintaining the temperature at 350°C for thirty minutes, the vessel was cooled, the pressure was released, and the product was removed. The reaction describing the hydrogen reduction of potassium perrhenate is

$$KReO_4 + 7/2H_2 = Re + KOH + 3H_2O \ .$$

The recovered product was washed thoroughly with hot distilled water and hot dilute hydrochloric acid in order to remove potassium hydroxide. The metal was further washed with 95 percent ethanol and vacuum dried at room temperature. The rhenium recovered after these treatments was submitted again to the entire reduction, washing, and drying processes in

order to increase the metal purity.

Although the rhenium metal powder obtained from potassium perrhenate was treated to extract potassium impurities, the complete removal of potassium was virtually impossible, even with repeated acid leaching. Therefore in order to obtain higher purity rhenium, workers at the University of Tennessee employed the hydrogen reduction of purified ammonium perrhenate. Rhenium metal, prepared from potassium perrhenate, was used as the starting material for the synthesis of purified ammonium perrhenate. The metal was placed in one end of a combustion tube and oxidized to Re_2O_7 at temperatures between 350° and 500°C. The oxide, volatile at these temperatures, sublimed away from the nonvolatile impurities and condensed on cool portions of the tube. The oxide was removed from the tube and reacted with distilled water to form perrhenic acid ($HReO_4$). The acid was neutralized with ammonia, and ammonium perrhenate crystals were collected, recrystallized twice, and dried. The dry ammonium perrhenate was placed in a quartz tube and reduced at 380°C in a mixed gas stream of hydrogen and nitrogen. The temperature was then raised to 700°-800°C and held at this temperature for one hour to insure complete reduction. The reaction describing the hydrogen reduction of

ammonium perrhenate is

$$NH_4ReO_4 + 7/2H_2 = Re + 4H_2O + NH_3 \ .$$

The rhenium metal powder prepared by this reduction procedure needed no further purification treatment since all products except the metal were volatile.

The Kennecott process (18,19)

Even though production of rhenium at the University of Tennessee was sufficient to meet domestic needs during the early 1950's, the use of molybdenite flue dusts as a source material made the over-all process very inefficient. Data obtained by the Kennecott Copper Corporation showed that more than ninety percent of the rhenium in molybdenite could be volatilized during roasting, however, only ten percent of the contained rhenium was normally associated with molybdenite flue dusts. In 1953 Kennecott initiated work on an alternate method of collecting rhenium during molybdenite concentrate roasting. Since the flue gases apparently contained most of the released rhenium, research efforts at Kennecott were directed toward the recovery of rhenium from the gases.

In the Kennecott process, gases and entrained particles from molybdenite roasting are directed into a hot-operated cyclone where most of the coarse flue dusts are separated from

the gases. The dusts are recycled to the roaster, and the exit gases from the cyclone are passed into a wet scrubbing tower. In the scrubbing tower, oxides of rhenium, molybdenum, and sulfur are extracted from the flue gases with water. The resulting solution is recycled through the scrubber a number of times in order to build up the concentration of rhenium. When the desired concentration has been obtained, the solution is bled from the scrubber and prepared for ion-exchange treatment by the addition of sodium hydroxide, sodium carbonate, and an oxidizing agent. Making the solution basic precipitates impurity metal hydroxides and favors selective adsorption of rhenium; the oxidizing agent raises rhenium and molybdenum to their highest valences; and carbonate facilitates separation of the insoluble hydroxides. The clean scrubber solution is then fed to a bank of ion-exchange columns. On passage through the columns most of the rhenium is adsorbed as perrhenate ion while much of the molybdenum and other impurities are not retained. Small amounts of molybdenum, held on the column, are successfully removed by elution with sodium hydroxide. After molybdenum impurities are removed, the adsorbed rhenium is stripped from the column with dilute perchloric acid. The rhenium-bearing solution is then reacted with hydrogen sulfide

to precipitate rhenium sulfide according to the reaction

$$HReO_4 + 7/2H_2S \rightarrow 1/2Re_2S_7 + 4H_2O \ .$$

The sulfide is recovered by filtration and digested with ammonium hydroxide and hydrogen peroxide to form a solution of ammonium perrhenate and ammonium sulfate. Ammonium perrhenate is then recovered by evaporation and selective crystallization. Further details of ammonium perrhenate purifications and treatments appear to be proprietary, but the production of rhenium metal powder essentially involves the hydrogen reduction of high purity ammonium perrhenate. By the process developed at Kennecott, almost ninety-five percent of the released rhenium is recovered, and a rhenium metal powder of 99.97^{+} (20) percent purity is produced.

Production and Costs of Rhenium

From 1930 until the outbreak of World War II the only commercial production of rhenium was conducted by W. Feit near Mansfield, Germany. Production capacity was approximately 120 kg of rhenium metal per year and the metal sold for about $2.40 per gram (17). Shortly after the start of World War II, domestic supplies of foreign rhenium metal were quoted at $15.00 per gram, however, when Melaven began small-scale production in 1942, the price of rhenium metal dropped to $10.00

per gram. With increased production in 1946, the price changed to between $6.00 per gram and $1.75 per gram, depending on the quantity and purity of the metal (21). Between 1942 and 1957 Melaven extracted about 300 pounds (17) of rhenium, as potassium perrhenate, from molybdenite flue dusts, and in 1955 the production capacity at the University of Tennessee was estimated at 50 to 60 kg per year (5).

The Chase Brass and Copper Company, Incorporated, a fabricating subsidiary of Kennecott Copper Corporation, is presently the major domestic supplier of rhenium metal and rhenium alloys. Chase Brass first offered rhenium metal powder for sale in 1955 at about $1.50 per gram for one half pound lots. In 1967 Chase Brass was offering 99.97^{+} percent rhenium metal powder at $1.30 to $1.45 per gram (20). In 1960 about 200 pounds of rhenium were produced in the United States, mostly by Chase Brass. By 1963 U.S. production approached 1400 pounds of which Chase Brass produced more than 1300 pounds (22). At present, Chase Brass is stockpiling rhenium in order to insure a stable supply to meet the needs of expanding markets.

Rhenium production is also carried out at foreign locations. Rhenium recovery is practiced in West Germany, England, and France, however, production appears to be small scaled and

primarily for laboratory usage (5,23). The Mansfield deposits have been reopened under East German control, and current production apparently exceeds the pre-World War II level (5). The U.S.S.R. initiated rhenium production in 1948 from molybdenite roaster flue dusts, and although production figures are not available, reasonable estimates place maximum Russian production at about 3000 pounds per year (24).

Some Uses of Rhenium (3,17,18,22)

A number of uses have been suggested for rhenium and rhenium compounds, but apparently the high cost and low production volume of rhenium have slowed down the development of commercial applications. One of the first applications of rhenium was in the manufacturing of pen points. Established applications for rhenium, however, are mostly in the lamp and electronic industries where use is made of the high melting point of rhenium (3180°C) (17) and its high temperature mechanical properties. The electrical resistivity of rhenium is about four times that of tungsten, a property that makes rhenium suitable for use as igniters for zirconium flash bulbs. A small amount of rhenium (3%) added to tungsten gives the igniter higher resistivity, greater strength, and improved shock resistance. Rhenium metal has replaced tungsten as a

filament in some mass spectrographs because rhenium is less affected by residual gaseous impurities. For the same reason, rhenium has also been used for ion gauge filaments. The ductility of rhenium, its high resistance to the water cycle effect, and the ability to use it in hydrogen, inert gases, and vacuum make rhenium attractive as a heater material for certain furnace and electronic tube applications. Since rhenium does not show a ductile-to-brittle transformation upon cooling, rhenium and some of its alloys are potentially useful for certain welding applications.

Another important high-temperature application of rhenium lies in temperature measurement. Thermocouples using combinations of W-3%Re vs. W-25%Re and W-5%Re vs. W-25%Re alloys are now being used for temperature measurements up to 2500°C. Rhenium also has physical and mechanical properties that are desired for electrical contact materials. Rhenium contacts resist mechanical wear, have high strength at elevated temperatures, and can withstand a variety of corrosive media. For some make-and-break contacts, such as telephone switching relays, rhenium offers improved resistance to arc erosion. Rhenium boats, crucibles, tubes, etc. have found considerable uses where the strength and corrosion resistance of rhenium are advantageous.

The catalytic uses of rhenium and some of its compounds are well established. As a catalyst, rhenium is relatively resistant to common poisons such as sulfur, selenium, phosphorus and many chlorides. Rhenium metal is an effective catalyst in dehydrogenating alcohols to aldehydes and ketones. Certain rhenium sulfides and oxides are employed for the selective hydrogenation of carbonyl or nitro groups, without attacking carbon-sulfur or carbon-halogen bonds. Studies also show that rhenium, supported on activated carbon or alumina, has high activity in hydro-cracking heavy hydrocarbon fractions to lighter distillates (25).

INVESTIGATION OF A MOLYBDENITE CONCENTRATE

Since most rhenium recovery methods are designed to collect the rhenium only as a by-product of molybdenite roasting, an alternate method for removing rhenium from the concentrate might be of interest. Exploratory experiments relating to the possibility of developing a method for the direct extraction of rhenium from a molybdenite concentrate have been performed, and some of the findings are reported here. Such a method might involve the separation of rhenium from the concentrate without molesting a significant amount of molybdenite. If an economical method for direct extraction could be developed, the recovery and production of rhenium might become less dependent on molybdenite considerations. Furthermore, if the method was very efficient, it might be applied to remove rhenium from primary molybdenite concentrates.

The amount of published information related to the direct extraction of rhenium from molybdenite concentrates is small. Lebedev (5) reported two unsuccessful attempts at the leaching of rhenium from molybdenite concentrates: by air oxidation at atmospheric pressure in a weakly alkaline medium and during oxidation by sodium hypochlorite. Most other publications pertaining to rhenium-molybdenite studies, however, are directed

toward the reaction of the whole concentrate followed by the chemical separation of rhenium and molybdenum. Since published accounts of direct extraction studies are apparently lacking, some exploratory tests of this investigation will be described in order to give others a possible basis for further work.

A Description of the Concentrate

Molybdenite, MoS_2, is the major constituent of rhenium-bearing molybdenite concentrates. It rarely occurs as well formed crystals but usually exists as soft thin platelets which have a greasy feel, metallic gray luster, and sometimes are mistaken for graphite. Molybdenite occurs in two similar structural forms (26), each having the physical appearance of graphite. The structure of the C-7 type hexagonal modification was reported by Dickinson and Pauling in 1923 (27), and the structure of the rhombohedral modification was correctly interpreted by Jellinek and others in 1960 (28). These structural forms are illustrated in Figure 1 where they are both referred to the same set of hexagonal axes for ease of comparison. Both modifications of MoS_2 are layer-type structures which can be described as the stacking of tri-layer units where each unit is composed of planes of S-Mo-S atoms. The

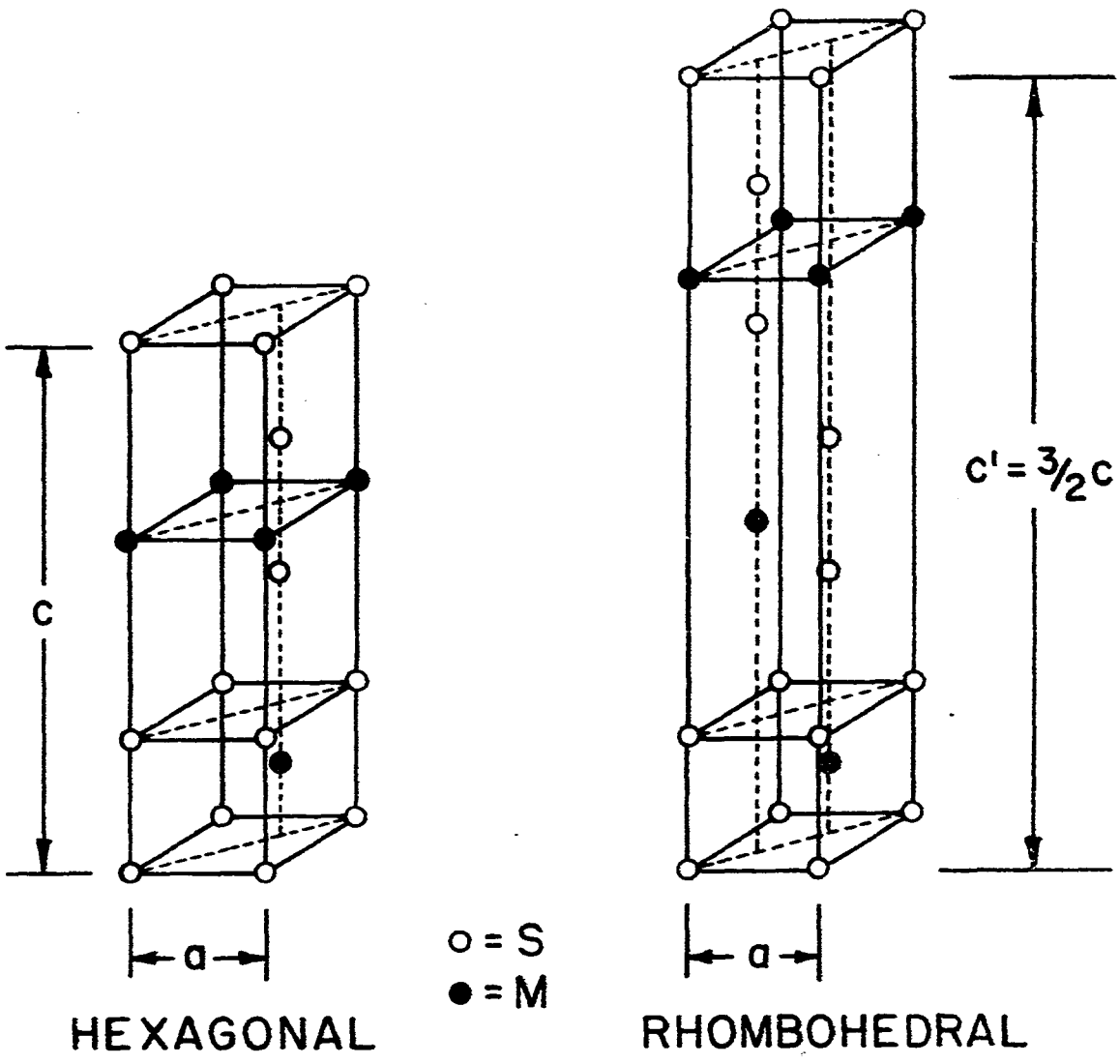

Figure 1. Two reported structural forms of MoS_2 and ReS_2

difference in the relative stacking arrangements between neighboring units accounts for the modifications of molybdenite. The measured unit cell parameters of the two forms of molybdenum sulfide and two forms of rhenium sulfide are presented in Table 2.

Table 2. MoS_2 and ReS_2 lattice parameters

Compound	Lattice type	a(Å)	c(Å)
MoS_2 (29)[a]	Hexagonal	3.160	12.295
MoS_2 (30)	Rhombohedral	3.16	18.37
ReS_2 (31)	Hexagonal	3.14	12.20
ReS_2 (32)	Rhombohedral	3.18	18.2

[a]Natural molybdenite, spectrographic analysis did not indicate a presence of rhenium.

Rhenium is only a minor constituent of certain molybdenite concentrates. The formal chemical composition of the rhenium fraction of the concentrates has not been determined explicitly, but a bisulfide is most likely. ReS_2 is a black solid which resembles MoS_2 in some of its properties. It is generally synthesized in an amorphous form, but disordered crystals will form at temperatures above 900°C. The structures of ReS_2 and MoS_2 appear to be very similar. Lagrenaudie (31)

reported that ReS_2 is isostructural with hexagonal MoS_2, but he did not present any data. Jellinek (32), citing his own unpublished work, could not unambiguously identify a hexagonal form of ReS_2, but he did report a rhombohedral form of the same structure type as rhombohedral MoS_2. The measured lattice parameters for the hexagonal and rhombohedral forms of MoS_2 and ReS_2 have been presented in Table 2.

Although the reported structures of ReS_2 appear to be closely related to the structures of MoS_2, the type of aggregation between the rhenium and molybdenite fractions of natural molybdenite concentrates has not been clearly established. The rhenium fraction might be contained in a phase that is separate from molybdenite, but it is also possible that the rhenium and molybdenite fractions are present as a single phase. Kagle (33) concluded from X-ray diffraction studies on various molybdenite concentrates that the rhenium sulfide is in solid solution with molybdenite, but this work is unpublished, and data to substantiate the conclusion are not available.

Materials

A commercial grade molybdenite concentrate was supplied by the Phelps Dodge Corporation. The concentrate was recovered

as a by-product from porphyry copper operations near Morenci, Arizona. The as-received concentrate was thoroughly mixed and shaken on a 150 mesh screen, U.S. Standard (105μ opening). Over 97.5 percent of the concentrate was -150 mesh, and this sieve fraction was used for exploratory tests. A summary of analytical analyses performed on the -150 mesh fraction is presented in Table 3a. The molybdenite fraction of this concentrate has the hexagonal structural form as determined by identification of the 103 and 105 reflections in X-ray powder diffraction photographs (26).

Table 3a. A summary of analytical analyses on -150 mesh molybdenite concentrate

Emission spectrographic analysis (Ames Laboratory)
Cu, Fe and Si are major impurities with trace amounts of Ag, Al, Ca, Co, Cr, Mg, Mn, Ti. No Re was detected.
Thermal neutron activation analysis (Ames Laboratory) (34)
Rhenium: 488 ± 20 ppm
Chemical analysis (Ames Laboratory)
MoS_2: 80.4% (analysis made for Mo)

All of the chemicals used in the exploratory tests were reagent grade unless stated differently elsewhere.

Exploratory Extraction Tests

Evaluation of exploratory tests

Neutron activation analysis was applied to evaluate the effectiveness of the exploratory tests performed on molybdenite concentrate. Analyses were performed by the Radiochemistry Group I of Ames Laboratory. The method (34), in part, employs the thermal neutron irradiation of the treated samples followed by sample dissolution, separation from interfering radionuclides, and counting of the low energy gamma radiation of Re^{186} and Re^{188}. This method gives accurate rhenium analyses to $\pm$ 5 percent or less.

In evaluating exploratory treatments for the selective removal of rhenium from the molybdenite concentrate, analyses for rhenium were made on the treated samples. The removal of 8 percent or more of the contained rhenium was applied as a standard for judging whether or not a treatment might be potentially worthwhile.

Solubility tests

The following chemicals were tested as solvents to determine if they would selectively dissolve rhenium from molybdenite concentrate: formic acid (90%), methanol, .25M triphenylphosphine in acetone, acetonitrile, dimethylsulfoxide,

N,N-dimethylformamide, diethylamine, tri-n-butyl phosphate, carbon bisulfide, piperidine, pyridine, and sodium polysulfide (2M Na_2S, 3M S). None of these solvents, as judged visually, appeared to interact with the concentrate, and neutron activation analysis did not indicate a selective removal of rhenium.

Selective solubility and reaction of the concentrate were also tested by separately refluxing portions of molybdenite concentrate in 10M NaOH, initially 12M HCl, 3M NaSCN in .1M HCl, 9M H_2SO_4, and elemental sulfur. The HCl and NaOH treatments, as judged visually, showed reaction with the gangue minerals to form yellow-green solutions; the thiocyanate treatment gave a faint blood red solution, possibly caused by iron in the gangue; and the sulfuric acid and sulfur treatments gave no visual evidence of reaction. When judged by neutron activation analysis, however, none of these treatments gave evidence of extracting rhenium.

Hydrolysis test

A portion of molybdenite concentrate was subjected to an autoclave treatment in order to test the possibility of hydrolysis. The concentrate was treated for 24 hours at 360°C (approximate pressure 2700 psi). The treated sample was removed, refluxed in initially concentrated HCl for four hours,

and then stirred for three hours in chlorine water[1]. A neutron activation analysis performed on the fully treated concentrate showed no appreciable depletion of rhenium by this series of treatments.

Selective oxidation tests

In the development of the extractive metallurgy of molybdenum, some processes employing various oxidizing agents have been devised for possible use in the dissolution of molybdenites found in waste dumps, tailing piles, and low-grade ores left in place. In consideration of a method for the selective leaching of rhenium from molybdenite concentrate, some of the conditions of these processes were considered in choosing reaction parameters for some exploratory tests. A typical test consisted of treating a portion of the concentrate under chosen conditions until a noticable portion had reacted, or until a suitable time had elapsed. Unused reagents and possible insoluble reaction products were removed from the treated concentrate before neutron activation analysis. The descriptions and experimental conditions for some tested exploratory oxidizing leaching treatments are presented in Table 3b.

---

[1] ReO_2 and $ReO_2 \cdot nH_2O$ form soluble $ReCl_6^{-2}$ in HCl and form soluble ReO_4^- in Cl_2 water.

Table 3b. A description of exploratory oxidation tests

Test no.	Oxidizing reagent and conditions	Further treatments or remarks
1[a]	Cl_2 continuously bubbled into distilled water, stir concentrate for about 10 hrs. at ~25°C	Insoluble H_2MoO_4 removed before analysis with 5M NaOH
2	-150 mesh MnO_2 in 7M H_2SO_4, stir concentrate for about 48 hrs. at ~70-80°C (35)	Unreacted MnO_2 removed with HCl before analysis
3[a]	1% H_2O_2 in 2M NaOH, stir concentrate for 15 hrs. at ~25°C (36)	None
4[a]	.3M HNO_3, stir concentrate for 15 hrs. at ~25°C	Insoluble H_2MoO_4 removed before analysis with 5M NaOH
5	.05% NaOCl in .12M Na_2CO_3, stir concentrate for 30 min. at ~25°C (37)	None
6	2M $FeCl_3$ in 2M H_2SO_4, stir concentrate for 24 hrs. at ~25°C	None
7[a]	.5M $Na_2S_2O_8$ in .5M H_2SO_4, stir concentrate for 12 hrs. at ~25°C	None
8	.5M $NaClO_3$ in .4M H_2SO_4, stir concentrate for 15 hrs. at ~25°C (38)	None

[a]This test was performed on a sample of -325 mesh concentrate in addition to the -150 mesh sample. There was essentially no difference in the extraction results.

Neutron activation analysis indicated that none of these treatments appeared to selectively leach rhenium from the molybdenite concentrate.

Vapor transport tests

The basic principles of vapor transport reactions have been discussed in detail by others (39,40). Transport reactions are generally those where a solid or liquid substance react with a gas to form only vapor phase reaction products which subsequently undergo a reverse reaction at a different place in the system. In addition to a reversible reaction, the system must have a concentration gradient which is often provided by maintaining a temperature differential. When these conditions are fulfilled, chemical transport of the solid or liquid substance might take place.

Halides MoS_2 undergoes transport ($950^{o}C \rightarrow 800^{o}C$) in the presence of chlorine (39), but the process has not been examined in detail. Published reports of ReS_2 transport reactions have not been found, but a rhenium dichlorosulfide, $ReSCl_2$, has been identified as an intermediate in the chlorination of ReS_2 (41). Solid $ReSCl_2$ appears to be stable in chlorine to $400^{o}C$ and chlorinates to $ReCl_5$ at 400^{o}-$450^{o}C$ (41). Since ReS_2 does form a stable chlorosulfide, it is possible

that a volatile transient iodosulfide might form between iodine and the rhenium fraction of molybdenite concentrate. Under the proper conditions this species might be transported away from molybdenite. It would be fortunate, however, if molybdenite would not react in an analogous manner.

In order to test the above proposal, a mixture of molybdenite concentrate and iodine were first sealed under vacuum in a 10 mm quartz tube. The mixture, shaken to one end of the tube, was then placed in the hottest region of a twelve inch long tube furnace, and the other end of the tube was allowed to extend out of the furnace. The cooler end of the tube was maintained at $130^{\circ} \pm 10^{\circ}C$ so that liquid iodine was in equilibrium with its vapor during the experiment. The hot end of the tube was first maintained at $500^{\circ}C$ for 72 hours, then at $650^{\circ}C$ for 72 hours and $800^{\circ}C$ for 72 hours, and finally at $1000^{\circ}C$ for 120 hours. After treatment, the tube was cooled rapidly and inspected visually for evidence of transport. There was no evidence for the transport of any appreciable quantity of material, and neutron activation analysis did not indicate a depletion of rhenium from the molybdenite concentrate.

Sulfur The existence of ReS_2 and Re_2S_7 are well estab-

lished and evidence of ReS_3 has been reported (6,42). Both higher sulfides reportedly lose sulfur at elevated temperatures and form ReS_2: Re_2S_7 above 500°C (42) and ReS_3 above 800°C (6). The reported instability of the higher sulfides suggests the possibility that a transport of ReS_2 might proceed through the following type of equilibrium

$$ReS_2(s) + xS(g) = ReS_{2+x}(g).$$

To test the possibility of this transport, a mixture of molybdenite concentrate and sulfur were manipulated in a manner analogous to the iodine treatment described above. The cooler end of the tube was maintained at 145° ± 10°C and the hotter end, containing the concentrate, was maintained first at 450°C for 72 hours, then at 550°C for 72 hours and 700°C for 72 hours and finally at 800°C for 90 hours. As with iodine, no transport appeared to take place, and no depletion of rhenium was indicated by analysis.

Discussion

The results obtained from exploratory extraction tests on a rhenium-bearing molybdenite concentrate indicated that rhenium and molybdenum reacted in proportion to their concentrations, therefore, selective extraction of rhenium was not obtained with the reactions tested here. From these results

it appears that the rhenium fraction is not present in a phase that is both separate from molybdenite and readily exposed for chemical reaction, however, a separate rhenium-bearing phase "embedded" in molybdenite and "shielded" by molybdenite from chemical attack can not be ruled out. A more detailed study of this possibility is presented in the next section.

Electron Microprobe Study

An electron microprobe study of the molybdenite concentrate was made to investigate the distribution of rhenium in more detail. This type of analysis employs an electron beam to excite the characteristic X-ray spectra of the elements in a sample. The characteristic X-rays of a particular element are then separated from the other X-rays, and the intensity, which is proportional to concentration, is recorded electronically. If the position of the electron beam on the sample is correlated with the position of an oscilloscope beam, and if the X-ray intensity is correlated with the intensity of an oscilloscope beam, then an image of the distribution of a particular element in a sample can be conveniently displayed.

Experimental procedure

A small amount of -325 mesh (44μ) molybdenite concentrate was mixed with aluminum metal powder, placed in a cylindrical

steel mold, and pressed with a plunger at room temperature at about 12,000 psi. The resulting solid wafer contained particles of concentrate dispersed throughout an aluminum matrix. The concentrate particles on one of the flat surfaces of the wafer were examined with an Applied Research Laboratory EMX Electron Microprobe X-ray Analyzer using a 30 keV excitation potential. The analyzer was set to detect molybdenum $L\alpha_1$ X-rays (5.4062 Å) and the sample was scanned for molybdenum content. The molybdenum image of the sample particles was displayed at 250X on an oscilloscope screen, and a Polaroid photograph was recorded in order to show the positions of the molybdenum-bearing particles. A similar scan measurement was made for the rhenium image using the $L\alpha_1$ X-ray line (1.4328 Å), and a Polaroid photograph was also recorded. A comparison of the two 250X photographs showed that the molybdenum sample image and rhenium sample image essentially matched. This indicated that rhenium and molybdenum appear evenly distributed throughout the individual molybdenite particles at 250X magnification.

The 250X photographs were used as a guide and some of the relatively large molybdenite particles were selected for further analysis at 1000X magnification. Scan measurements

were made on selected particles and some photographs were recorded. The photograph displayed at the top of Figure 2 shows a 1000X molybdenum image of a typical molybdenite particle, and the photograph at the bottom of Figure 2 shows the rhenium image of the same particle. The important feature of these photographs is the even distribution of both rhenium and molybdenum throughout the particle at 1000X.

In addition to the scan measurements displayed in Figure 2, a series of stationary measurements was made on some of the larger molybdenite particles. A single stationary measurement consisted of exciting the sample with a stationary electron beam and counting the number of rhenium $L\alpha_1$ photons that reached the detector during a forty second time interval. A series of stationary measurements on one particle consisted of a number of single stationary measurements, usually fifty or more, made at intervals of one micron across the sample in a pattern of an "X". The data obtained from a series of stationary measurement on a typical molybdenite particle is presented as a frequency histogram in Figure 3. The values plotted along the abscissa represent the approximate concentration of rhenium in ppm (the observed concentration data contained a fourth significant figure not included here). The values plotted

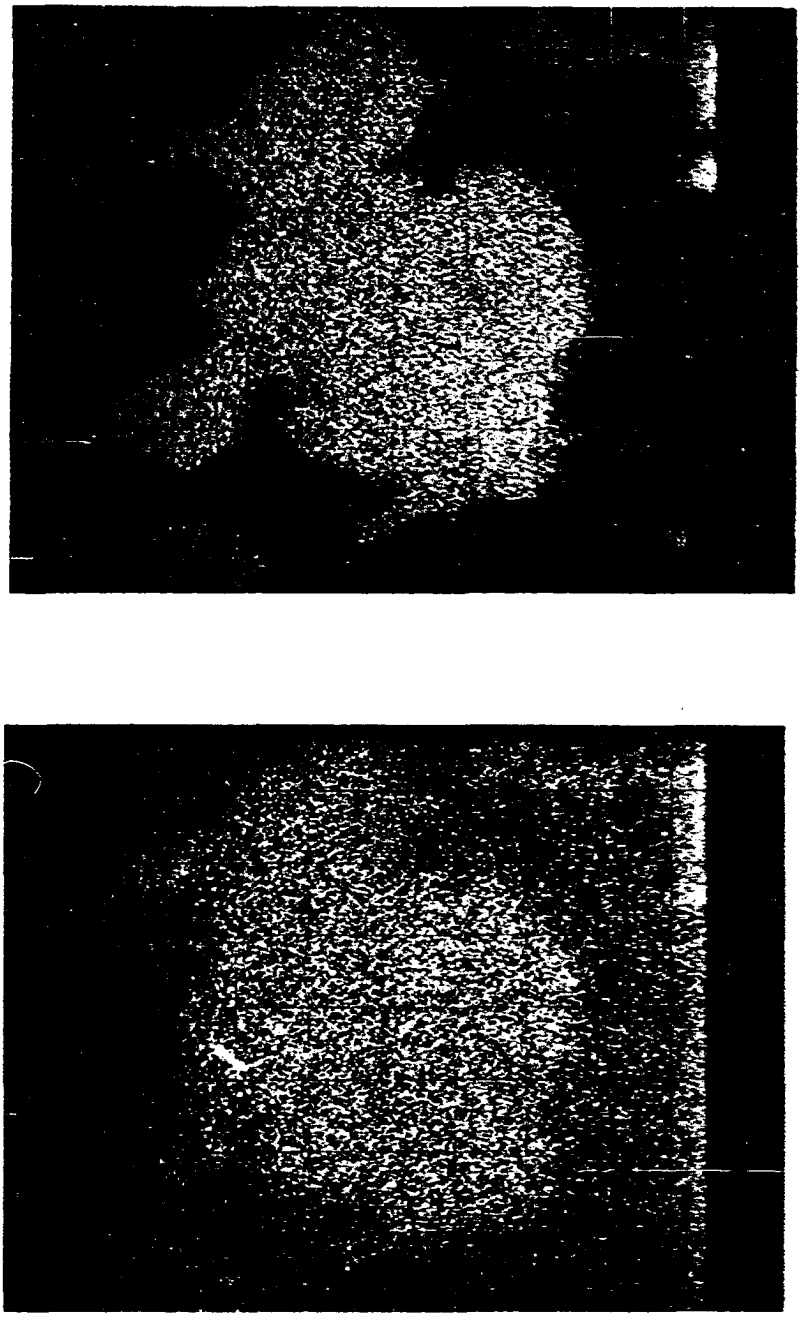

Figure 2. Electron microprobe image of a typical molybdenite particle
Top - Molybdenum image (1000X)
Bottom - Rhenium image (1000X)

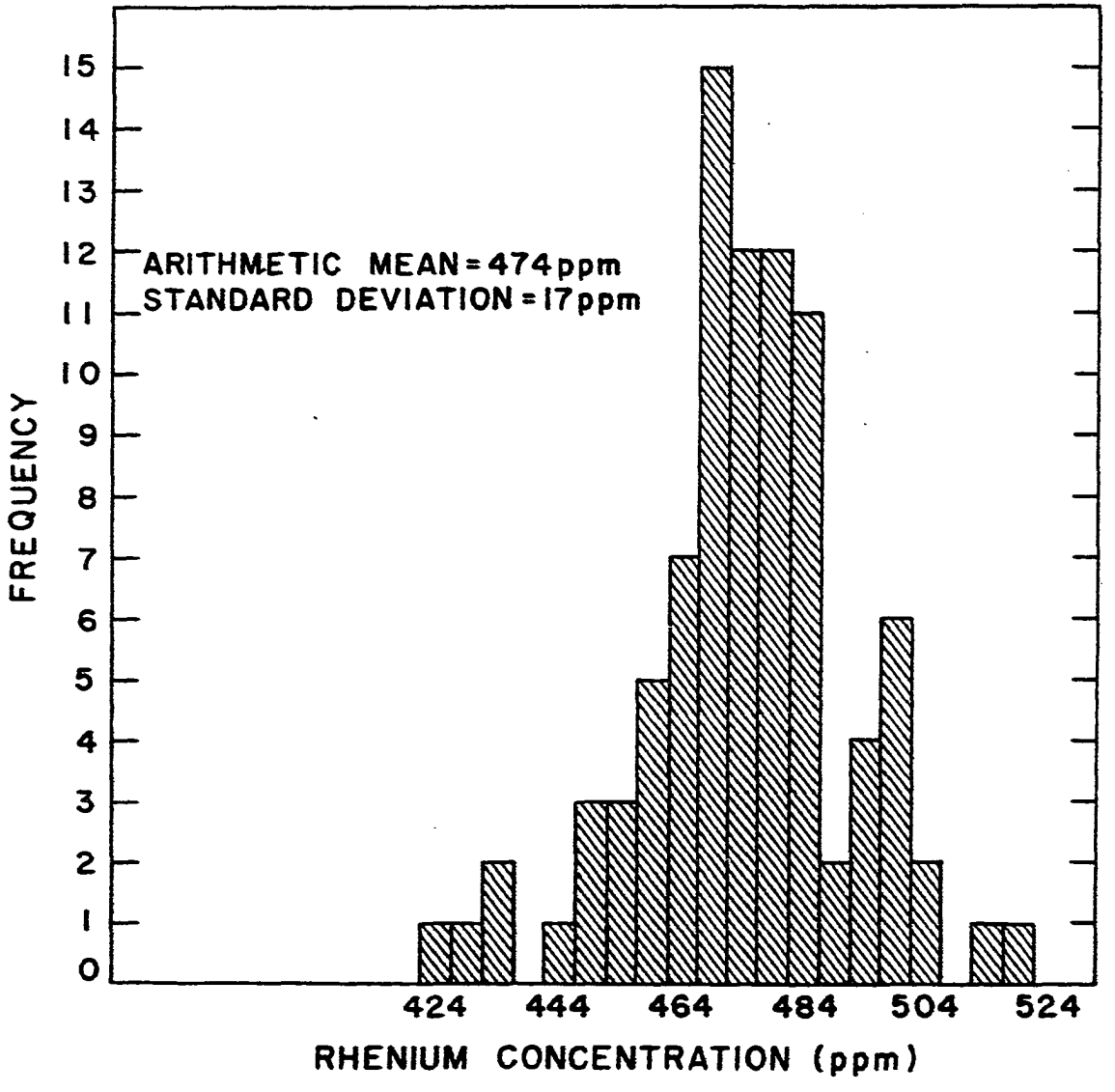

Figure 3. A frequency histogram of the rhenium distribution in a typical molybdenite particle

along the ordinate represent the number of times out of eighty-nine measurements that a particular rhenium concentration was observed. The arithmetic mean of the observed rhenium concentration is 474 ppm with a calculated standard deviation of 17 ppm. The median is also 474 ppm and the maximum observed deviation from the arithmetic mean is 11 percent.

Discussion

The photographs of Figure 2 allow a convenient visual 1000X examination of the rhenium and molybdenum distributions in a typical molybdenite particle, but further quantitative treatment of data gathered in this form is not readily accomplished. The numerical data presented in the frequency histogram, however, is quantitative and can be examined more closely.

In order to analyze the histogram data more completely, a further description of some of the measurement parameters is necessary. The electron beam is approximately .3μ in diameter as it approaches the sample, but the electrons are influenced by sample topography and they generally scatter on impact to give an effective beam size of .6-.7μ. After a 30 keV beam has penetrated 4μ into molybdenite, only about one percent of the electrons will retain enough energy to ionize rhenium (8.65

keV). If it is assumed, therefore, that the effective beam size is .7μ in diameter and the average depth of beam penetration is 3μ,[1] then each measurement represented in Figure 3 was made on an effective volume of about $1.15\mu^3$ (about 2×10^{10} MoS_2 formula units).

If the irradiated volume is considered to represent an effective sampling size, then a correlation can be made between the experimental data and a statistically treated model. Since solid solution and a separate "embedded" rhenium-bearing phase are the two possibilities being considered for the distribution of rhenium, it is worthwhile to establish a numerical relationship between experimental data and a model of the "embedded" phase. An answer to the following question could be meaningful: If it is supposed that all of the rhenium is contained in a separate "embedded" phase, and this phase is evenly distributed throughout the molybdenite phase, what is the largest average size that can be assigned to the fragments of the rhenium-bearing phase and still be consistent with the observed distribution of data? In order to answer this question, the

[1]Although 99% of the electrons will have lost their ionizing ability at a depth of 4μ, the electrons lose their energy approximately as an exponential function of depth, therefore the assumption of 3μ as the effective beam penetration is reasonable.

following are considered:

1) The calculated arithmetic mean and the median for the data of Figure 3 are equal, and the shape of the distribution histogram is nearly symmetric, therefore, the observed data is assumed to follow a normal distribution.

2) Statistical counting errors, possible real variations in the distribution of rhenium, and irregularities in the surface of the sample will all contribute to differences between the measured rhenium concentration and the average rhenium concentration. For this calculation, however, the differences between measured and average rhenium concentrations are assumed to arise only from fluctuations in the distribution of the supposed "embedded" phase.

3) Each "embedded" fragment is treated as a cube, and the entire molybdenite particle is considered to be made up of perfectly stacked and equally sized rhenium cubes and molybdenum cubes.

4) N is defined as the irradiated volume of the sample divided by the volume of one cube. It represents the number of cubes in the irradiated volume.

5) The model of the "embedded" phase in molybdenite consists of a population of randomly distributed molybdenum cubes and rhenium cubes that are represented in proportion to the

atom concentrations of molybdenum and rhenium. The statistical treatment pertains to sampling N cubes from this population and counting the rhenium cubes. If a large number of samplings, N cubes each time, are made from this population, then the sampling data should follow a normal distribution. For a particular ratio of rhenium to molybdenum cubes, the standard deviation (square root of the variance) of the mean rhenium concentration should depend on N, therefore, if the statistically calculated mean and variance of this model are correlated with the distribution of data in Figure 3, a value can be obtained for N and the cube size can be calculated.

6) Each sampling of N cubes is considered to be made from a population where the ratio of molybdenum to rhenium cubes is the same for each sampling. The treatment of a large number of samplings will then be according to the binomial distribution. This treatment is justified upon consideration of the observed data presented in Figure 3 and the assumption of item 1) above.

A mathematical treatment of the model described above is summarized in Table 4. This indicates that rhenium could be present in molybdenite as a finely divided phase with an average fragment size of 90 Å or less. For this treatment it was

Table 4. A summary of a statistical fragment size calculation

474 ppm Re in molybdenite concentrate that is eighty percent MoS_2 gives a 1:2,000 atom Re:Mo ratio.

Therefore:

Probability of rhenium = $5 \times 10^{-4} \equiv p$

Probability of molybdenum $\simeq 1 \equiv q$

For samples consisting of N cubes:

Expected mean rhenium concentration = $pN = 5 \times 10^{-4}N$

Expected variance in the mean rhenium concentration = $pqN = 5 \times 10^{-4}N$

The expected mean and variance are proportional (K) to the observed mean and variance for Figure 3.

$474K = 5 \times 10^{-4}N$

$(17)^2K^2 = 5 \times 10^{-4}N$

$N = 1.56 \times 10^6$ cubes

Volume of cube = beam volume/N = $7.37 \times 10^5 \text{Å}^3$

$a = (\text{volume})^{1/3} = 90\text{Å}$

assumed that the spread in the observed rhenium concentration data resulted only from fluctuations in the distribution of the "embedded" phase throughout molybdenite (item 2) above), however, if possible experimental errors are considered, the

calculated fragment size would be reduced. Therefore, when the calculated fragment size and the similar structures and lattice parameters of MoS_2 and ReS_2 are considered together, it seems very reasonable to conclude that the rhenium and molybdenum fractions of this molybdenite concentrate are associated as a solid solution.

IDENTIFICATION OF A WHITE RHENIUM OXIDE

Background

Since the discovery of rhenium in 1925, the oxides have probably been among the most often studied rhenium compounds. At least eight different rhenium oxides have been reported, but only three oxides are well characterized: ReO_2, ReO_3, Re_2O_7. Rhenium dioxide has been prepared by the high temperature reduction of ReO_3 or Re_2O_7 with either rhenium metal or hydrogen. The dioxide is a dark brown solid that crystallizes in orthorhombic and monoclinic structural modifications (43), and it readily oxidizes to either Re_2O_7 or perrhenate ion under appropriate conditions. Rhenium trioxide is a red cubic crystalline solid (44) that is commonly prepared at elevated temperatures by the reduction of Re_2O_7 with either carbon monoxide, rhenium dioxide, or rhenium metal. It can also be synthesized by pyrolysis of a Re_2O_7-dioxane complex. ReO_3 does not react with hydrochloric acid or dilute alkali, but it dissolves in nitric acid or hydrogen peroxide to form the perrhenate ion. ReO_3 exhibits metallic conductivity (45).

Rhenium heptoxide is the most common rhenium oxide. It is readily formed by heating rhenium in air or oxygen. Powdered rhenium metal begins to oxidize at about 160°C, and the

oxidation of massive metal begins at about 600°C (46). Oxidation proceeds through intermediary lower oxides, red ReO_3 being observable on the rhenium metal surfaces. The heptoxide is a yellow solid belonging to the orthorhombic crystal system. The crystal structure (47) consists of double layers of Re_2O_7 polymeric chains where the double layers have only van der Waals contacts to neighboring layers. Within a double layer, rhenium exhibits alternating tetrahedral and octahedral coordinations with the oxygens. The asymmetric unit of the Re_2O_7 crystal structure is illustrated in Figure 4 along with the appropriate bond distances.

Re_2O_7 usually sublimes at temperatures above 250°C, but in a sealed tube it melts at about 300°C. The melting and boiling points obtained from vapor pressure measurements are 300.3°C and 360.3°C respectively (48). The vapor phase consists of Re_2O_7 monomers with rhenium showing tetrahedral coordination with the oxygens (47). The heptoxide is extremely hygroscopic and readily dissolves in water to give perrhenic acid; the reaction is reversible and Re_2O_7 can be recovered by appropriate treatments.

Among other reported rhenium oxides is a white smoke-like material whose composition and behavior have not been well

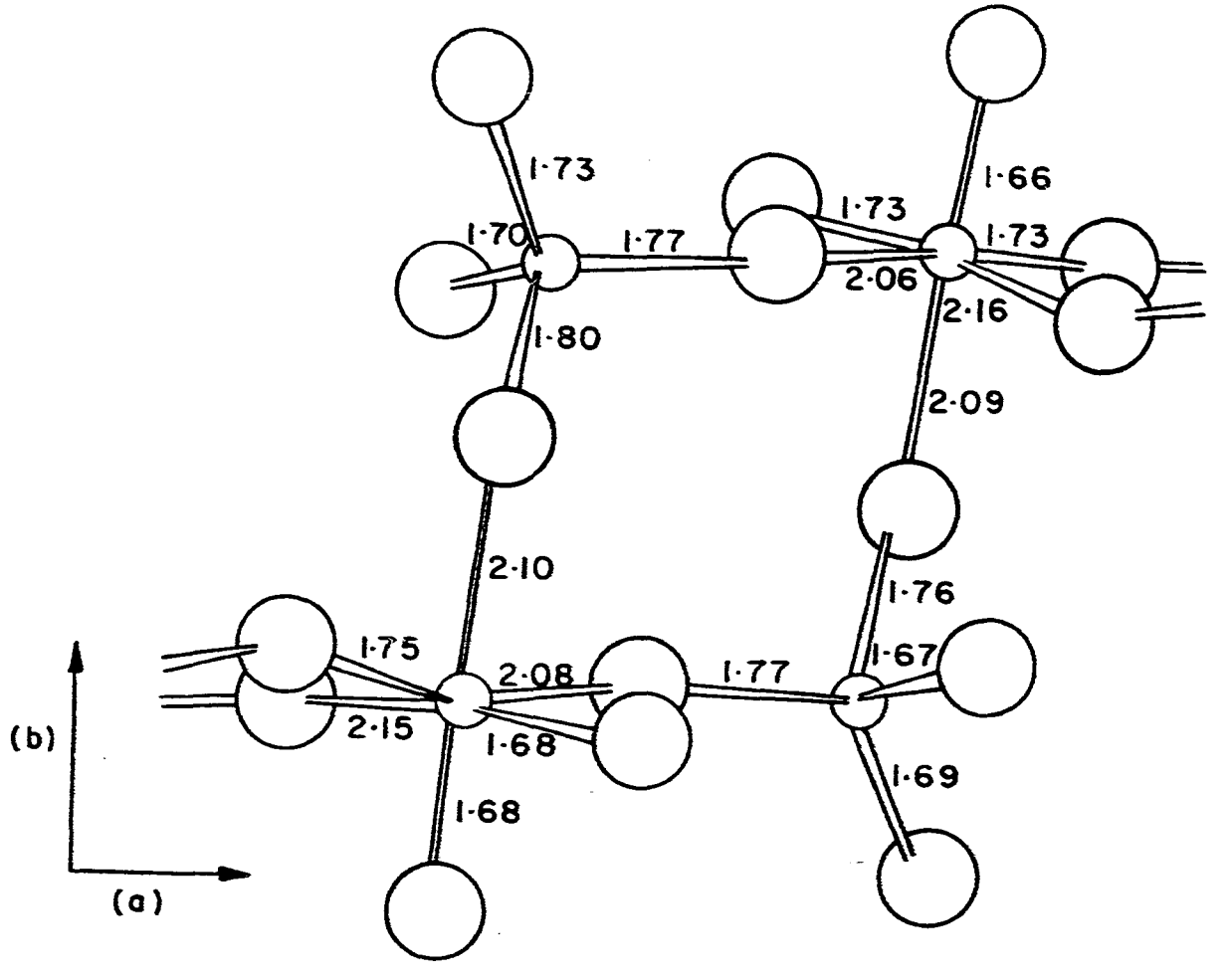

Figure 4. The asymmetric unit of the Re_2O_7 structure along with bond distances in Å (47)

characterized. The Noddacks were the first to report this oxide (49,50,51). The oxide was formed along with Re_2O_7 when a stream of cool oxygen gas (temperature below 150°C) was passed over the hot surface (about 300°C) of either rhenium metal powder or other rhenium oxides. The resulting white substance was described by the Noddacks as very small droplets that eventually deposited on the cool walls of the apparatus as a kind of snow. The solid white oxide was reported to decompose into Re_2O_7 and oxygen, gradually at room temperature and rapidly at elevated temperatures. It dissolved in acidic and basic solutions and melted at about 150°C. The reported chemical analyses indicated a greater oxygen to rhenium ratio than in Re_2O_7. The white oxide was reported to color acidic titanate and vanadate solutions yellow and discolor acidic permanganate solution, reactions which are characteristic of peroxide. The observed chemical behavior and the position of rhenium in group seven of the periodic system led the Noddacks to interpret the white oxide as a peroxide, and they assigned it the formula Re_2O_8.

Ogawa (52) measured the vapor pressure of Re_2O_7 and the total pressure over the white oxide as functions of temperature. Measurements made on Re_2O_7 between 230°C and 360°C

indicated an equilibrium between vapor and solid or liquid oxide, depending on the temperature in question. Pressure measurements on the white oxide, however, indicated the dissociation reaction

$$2Re_2O_8 \rightarrow 2Re_2O_7 + O_2 \ . \qquad (1)$$

Ogawa corrected the measured pressures for oxygen contributions and derived the vapor pressure of Re_2O_8 for temperatures between 100°C and 220°C. The reported vapor pressure ranged from 6.6 mm at 100°C to 46.6 mm at 220°C, substantially higher than the vapor pressure of Re_2O_7 (3 mm at 230°C). Ogawa also observed the white oxide was very difficult to collect. During one phase of oxide preparation, Ogawa noted that the oxide passed directly through a series of four sulfuric acid bubblers which were used to keep moisture out of the system.

Briscoe and others (53) investigated the rhenium oxides and concluded Re_2O_7 was the highest oxide. They showed that moisture could lower the melting point of the heptoxide to about 150°C and suggested that the alleged Re_2O_8 was either a modification of Re_2O_7 or wet Re_2O_7. Hagen and Sieverts (54) also studied the white material, and although they observed the conversion of white oxide to yellow oxide upon heating,

their experiments did not confirm the dissociation reaction reported by Ogawa (Equation 1). Druce (6) reported the work of the Noddacks but doubted the existence of Re_2O_8. Tribalat (55), however, reported that white fumes of rhenium oxide could be formed from Re_2O_7 is a current of oxidizing gas, but she dismissed the possibility of a higher oxide or an allotropic state of Re_2O_7. She described the white fumes as a spray of perrhenic acid resulting from the reaction of heptoxide with moisture impurities in the gas stream. Woolf (56) and Peacock (57) agreed with Tribalat, and these authors emphasized the difficulty of collecting the white material. Colton (58), however, classified the white substance as a very fine smoke which is extremely difficult to condense.

Some investigators interested in the extractive metallurgy of rhenium have also reported a rhenium containing material that closely resembles the white oxide. Sargent (59) wrote that the concentration of rhenium in molybdenite roaster flue dusts at the Miami Copper Co. dropped from 10,000-15,000 ppm to about 3,800 ppm when the molybdenite roasting temperature was raised. He observed that some of the "volatile Re_2O_7" passed through the cyclone precipitator and went "up the stack in a white, foglike vapor...".

Lebedev (60), in discussing the recovery of rhenium from molybdenite roaster flue gases, stated that "under favorable conditions rhenium oxides condense in the form of a smoke of particle size up to 10^{-4}-10^{-5} cm. The removal of such particles by gravity separation in dust chambers or by centrifugal separation in cyclones is wholly ineffective, and methods based on filtration, electrodeposition or gas washing have to be applied".

The experiments to be described in this section pertain to the white rhenium material. The need for this study is apparent, both from a basic and applied standpoint. A basic understanding of the nature and identity of the white substance would contribute to the knowledge of rhenium chemistry and might lead to improvements in the extractive metallurgy of rhenium.

Experimental

Preliminary studies of the white material were carried out to determine the significance of certain experimental parameters. These findings were then used in designing experiments for more detailed studies.

A modification of the method of Melaven and others (61) was employed to synthesize dry Re_2O_7 for use as a starting

material in making the white oxide. A line drawing of the Pyrex glass apparatus employed to make Re_2O_7 is presented in Figure 5. Rhenium metal powder of 99.97^+ percent purity was placed in the sealed end of a Pyrex glass tube, and the open end was joined to the manifold of the oxygen ballast system. The whole apparatus was slowly evacuated, with care being taken to prevent rhenium from dispersing throughout the system as a result of rapidly out-gassing the fine powder. With the exception of the area adjacent to the rhenium, the entire system was flamed under vacuum to drive out adsorbed water. With the system still under vacuum, a furnace was placed around the end of the tube containing the rhenium, the furnace temperature was slowly raised to 450°C, and the rhenium metal powder was baked under vacuum for 24 hours. During baking, the entire system was periodically flamed to insure complete dryness. When the baking step was completed, the vacuum line was closed, and the furnace was removed to allow the rhenium to cool. Extra dry grade oxygen was introduced into the system through a drying column of Linde 3A molecular sieves, and a tube furnace, preheated to 425-450°C, was positioned between the rhenium powder and the manifold. The hot furnace was moved in small increments toward the rhenium powder which

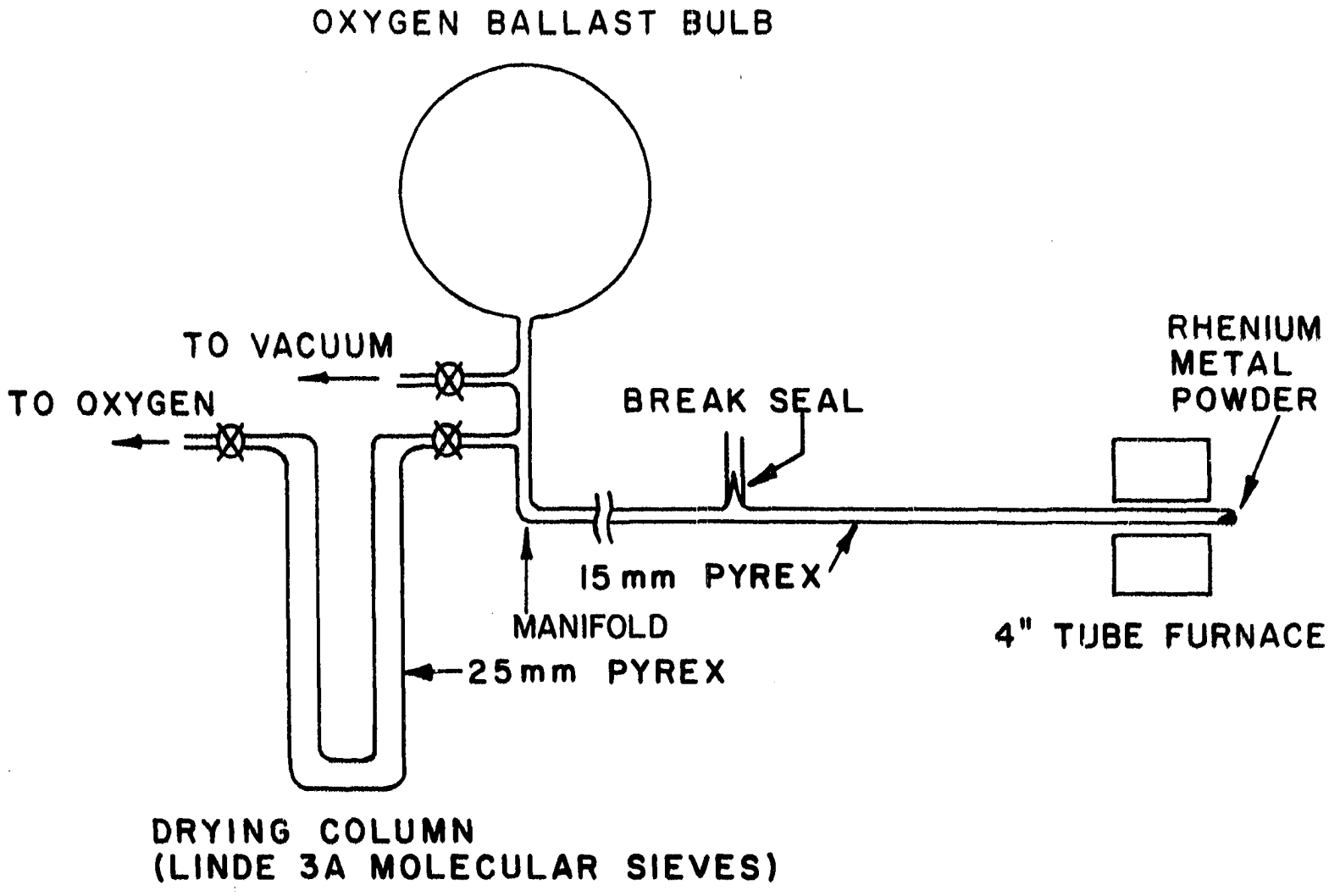

Figure 5. A representation of the apparatus used to prepare dry Re_2O_7

oxidized readily to Re_2O_7. The resultant heptoxide sublimed through the hottest zone of the furnace and deposited as a yellow crystalline solid between the furnace and the manifold. After all of the rhenium had oxidized, the furnace was removed and the emptied end of the tube was sealed off from the rest of the system. The above procedure was repeated at least two more times to insure complete oxidation to Re_2O_7 and allow the oxide to sublime away from any nonvolatile impurities. After a final sublimation, the tube containing the heptoxide was sealed off from the manifold. The apparatus was designed so the capsulated oxide would then be accessible through an attached glass break seal. The break seal permitted further manipulation of the oxide without exposing it to possible moisture contamination. This method was routinely applied to oxidize from one to ten grams of rhenium powder, with three grams the most common amount. Oxide prepared by this method melted in a sealed tube at $301^{\circ} \pm 1^{\circ}C$.

The white material was prepared by two methods: 1) passing a cool dry gas stream over heated rhenium heptoxide, 2) passing a cool dry oxygen stream over heated rhenium metal powder. Preliminary experiments indicated that a white substance formed readily in a dry gas stream, therefore, in order

to eliminate the moisture variable, special precautions were taken to dry the incoming gas. It was first passed through a four foot long column of freshly regenerated Linde 3A molecular sieves and then directed into a cold trap. In addition to drying the gas, the cold trap also cooled the gas. A line drawing of the Pyrex glass apparatus used for the preparation and collection of the white oxide is shown in Figure 6.

To make the white oxide from Re_2O_7, sealed ampoules of heptoxide were prepared as previously described and attached through a break seal as illustrated in Figure 6. The break seal was not broken until the apparatus was first flamed under vacuum to remove adsorbed water. After the break seal was broken and a gas stream was flowing through the system, the entire ampoule and the tube connecting the ampoule to the main flow tube were heated to and held at 300°C. (The vapor pressure of Re_2O_7 at 300°C is 160 mm.) The white oxide formed as the flowing gas stream mixed with the heptoxide vapors at the junction of the connecting and main flow tubes. The oxide remained in suspension in the carrier stream and passed with the stream into the spiral condenser which was cooled by a dry-ice-methanol bath to about -78°C. Yellow Re_2O_7 deposited on the condenser walls, but most of the white oxide passed

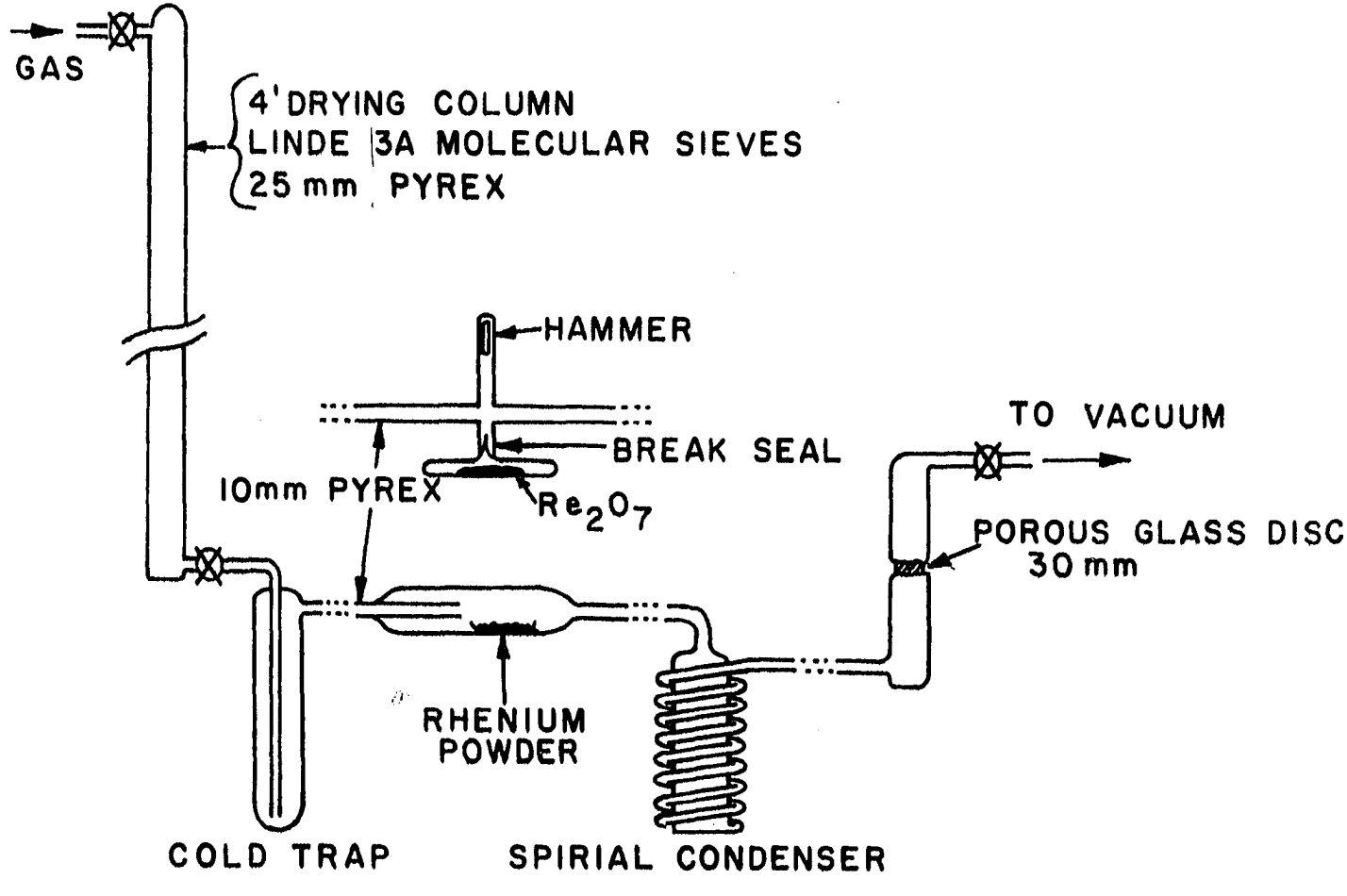

Figure 6. A representation of the apparatus used to prepare the white rhenium oxide

through. The gas stream exiting from the spiral condenser was used directly for experiments requiring the suspended form of oxide. For analyses and experiments requiring bulk quantities of the oxide, the exit tube of the spiral condenser was connected onto a sealing tube constructed with a 30 mm medium size porous glass disc (porosity 10-15μ). The gas stream was drawn through the disc to collect the suspended white oxide.

In the preparation of white oxide from rhenium metal, the apparatus was essentially as described above except for the reaction chamber and the materials. As illustrated in Figure 6, rhenium metal powder of 99.97+ percent purity was placed in a quartz boat beneath the gas flow tube. Before oxidizing the metal, the entire system was flamed under vacuum, and the rhenium metal powder was baked in place at 450°C for 24 hours under vacuum. The reaction chamber containing the rhenium was then cooled to 310°-320°C and maintained at this temperature while cool dry oxygen was passed over the rhenium to produce the white oxide. The yellow heptoxide that also formed during oxidation deposited in the spiral condenser, and most of the white oxide passed through. The condenser exit stream was handled as previously described.

Three different gases were studied in preparing the white oxide. Oxygen, nitrogen, and helium[1] were investigated in conjunction with rhenium heptoxide, and oxygen was studied with rhenium metal powder. All three gases were found to produce the white oxide. When studies were made with nitrogen or helium, the cold trap was filled with liquid nitrogen (-196°C). Oxygen condenses at the liquid nitrogen temperature, therefore, for oxygen studies the cold trap was filled with an isopentane slush (-161°C). For all three gases, variations in flow rate above 300-350 cm^3/min did not appreciably effect white oxide formation, although yields were substantially reduced for rates below this range. The reduced yields probably resulted because the flowing gas stream was too slow to sweep the heptoxide from the heated regions fast enough to cool it rapidly and convert it to white oxide.

Rhenium analyses were made on samples of white oxide prepared by both methods and collected on a porous glass disc. A gravimetric procedure was used whereby a weighed portion of oxide was dissolved in water and precipitated by tetraphenylarsonium chloride. The precipitate was weighed as $(C_6H_5)_4AsReO_4$ (62). The oxygen content was determined by difference.

[1]Extra Dry Grade oxygen, Extra Dry Grade nitrogen, 99.9999 percent helium.

The results of these analyses and analyses on yellow crystalline Re_2O_7 are presented in Table 5. The analyses show that the white rhenium oxide essentially has the composition Re_2O_7.

Table 5. Analyses of yellow and white rhenium oxides

Description	Reactants	Oxide weight (gm)	$(C_6H_5)_4AsReO_4$ weight (gm)	Determined oxide formula
Yellow Re_2O_7	O_2, Re	.7501	1.9758	$Re_2O_{6.76}$
		1.0951	2.8455	$Re_2O_{7.18}$
		1.0350	2.7170	$Re_2O_{6.86}$
White oxide	O_2, Re	.5686	1.4843	$Re_2O_{7.04}$
		.5802	1.5085	$Re_2O_{7.16}$
		.5438	1.4178	$Re_2O_{7.08}$
	O_2, Re_2O_7	.8517	2.2383	$Re_2O_{6.88}$
		1.2382	3.2206	$Re_2O_{7.16}$
	N_2, Re_2O_7	.6043	1.5666	$Re_2O_{7.26}$
		.8050	2.0809	$Re_2O_{7.34}$
	He, Re_2O_7	.9273	2.4392	$Re_2O_{6.82}$

Experiments were performed on bulk and suspended forms of white oxide. When the exit gas stream containing the suspended oxide was bubbled separately into water, 2M NaOH, and 2M HCl, the oxide was not appreciably retained but passed on through the solutions. A quantity of suspended oxide was

trapped in a flask containing two electrodes positioned an eighth inch apart as capacitor plates. When the electrodes were charged to 1000 V D.C., the oxide appeared unchanged and showed no movement toward either electrode. Another quantity of the suspended oxide, made from Re_2O_7 and oxygen, was trapped and enclosed in a flask where it remained in suspension for about 24 hours; it eventually deposited as a thin layer on the walls of the flask. A photomicrograph of an area of the deposited layer is shown in Figure 7. The small white dots are dispersed oxide particles. The fuzzy large white areas are aggregates of smaller particles. The structure of the aggregates has the appearance of fluffy balls of cotton.

The oxide in bulk form reacted with water to give an acidic solution, but no bubbles were evolved and the solution did not discolor permanganate. A vessel containing white oxide was evacuated, sealed and heated to 250°C. The oxide did not appear to melt but transformed to yellow heptoxide at about 125°-150°C. The yellow heptoxide remained after cooling the vessel. A mass spectrum of the gas in the cooled vessel showed no oxygen above background levels.

The near infrared spectrum of the white oxide was ob-

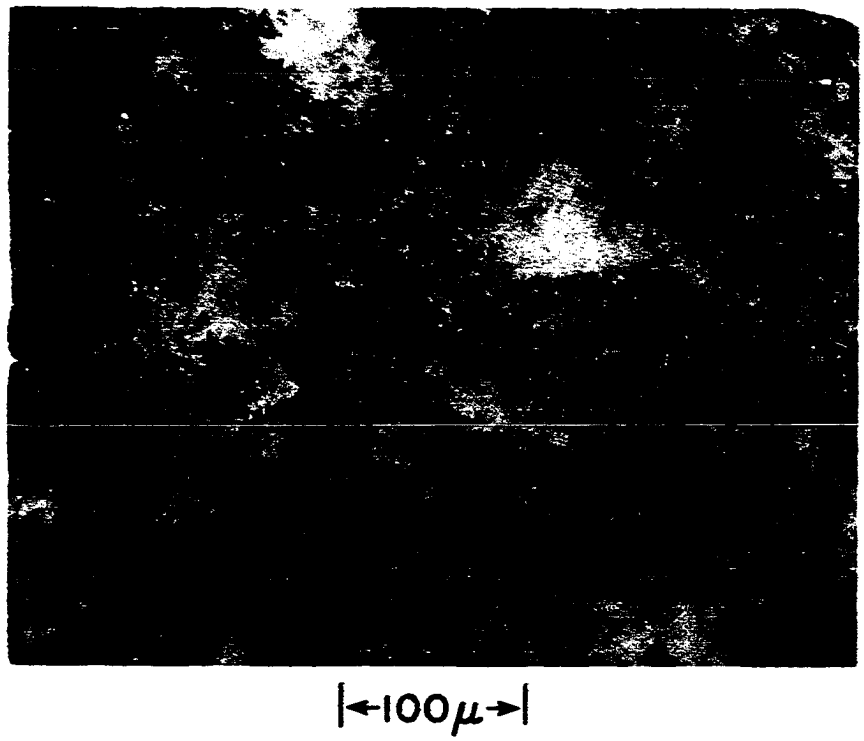

Figure 7. A photomicrograph of an area of a deposited layer of white rhenium oxide

served in a Nujol mull and found to agree closely with the spectrum of yellow Re_2O_7. Both spectra showed a broad absorption band between 800 cm^{-1} and 1000 cm^{-1} with the broad band of the white oxide shifted slightly (10-15 cm^{-1}) to higher energy.

In order to check on the dissociation reaction reported by Ogawa (Equation 1), the pressure over a sample of the white oxide was measured as a function of temperature between 75°C and 275°C. A diaphragm gauge of the type described by Berry (63) was used as a null instrument and pressures were read from a closed end mercury manometer to $\pm$ 0.5 mm. No pressure was observed at temperatures below 200°C, but pressures of 2 mm, 9.5 mm, and 52.5 mm were recorded at 223.1°C, 247.4°C, and 276.9°C respectively. These values agree closely with the measured vapor pressures of yellow Re_2O_7 (48,52).

Freshly prepared white oxide, made from Re_2O_7 and oxygen, was packed into thin-walled Lindermann glass capillaries (0.2 mm diameter) and examined by X-ray powder diffraction techniques. Twenty-four hour exposures were made with nickel filtered copper K_α radiation in a large Debye-Scherrer camera. The observed X-ray pattern consisted of a single low intensity diffraction band. The same samples were then annealed in the

capillaries at about 50°C for 20 hours, re-examined by X-rays, and found to exhibit a very intense sharp-lined diffraction pattern. The pattern was characteristic of crystalline Re_2O_7. Superimposed densitometer tracings illustrating the degree of darkening of the broad band and sharp-lined diffraction photographs between 20° and 31° in two theta are presented in Figure 8. The correspondence between the white oxide diffraction band and the indexed diffraction peaks of Re_2O_7 has not been specifically established, however, if the white oxide is assumed to be a finely divided form of rhenium heptoxide, then X-ray line broadening theory can be applied to calculate an approximate value for the average crystallite size. This calculation (see Appendix A) indicates the average crystallite size of the white oxide is approximately 20Å.

Discussion

On the basis of the evidence presented above it appears that the white rhenium material is a rhenium heptoxide smoke. Evidence for the proposed peroxide and perrhenic acid descriptions has not been established. The dry synthetic conditions and the chemical analyses do not support the perrhenic acid description. Likewise, chemical analyses, the ability to make the oxide with nitrogen and helium, and absence of a charac-

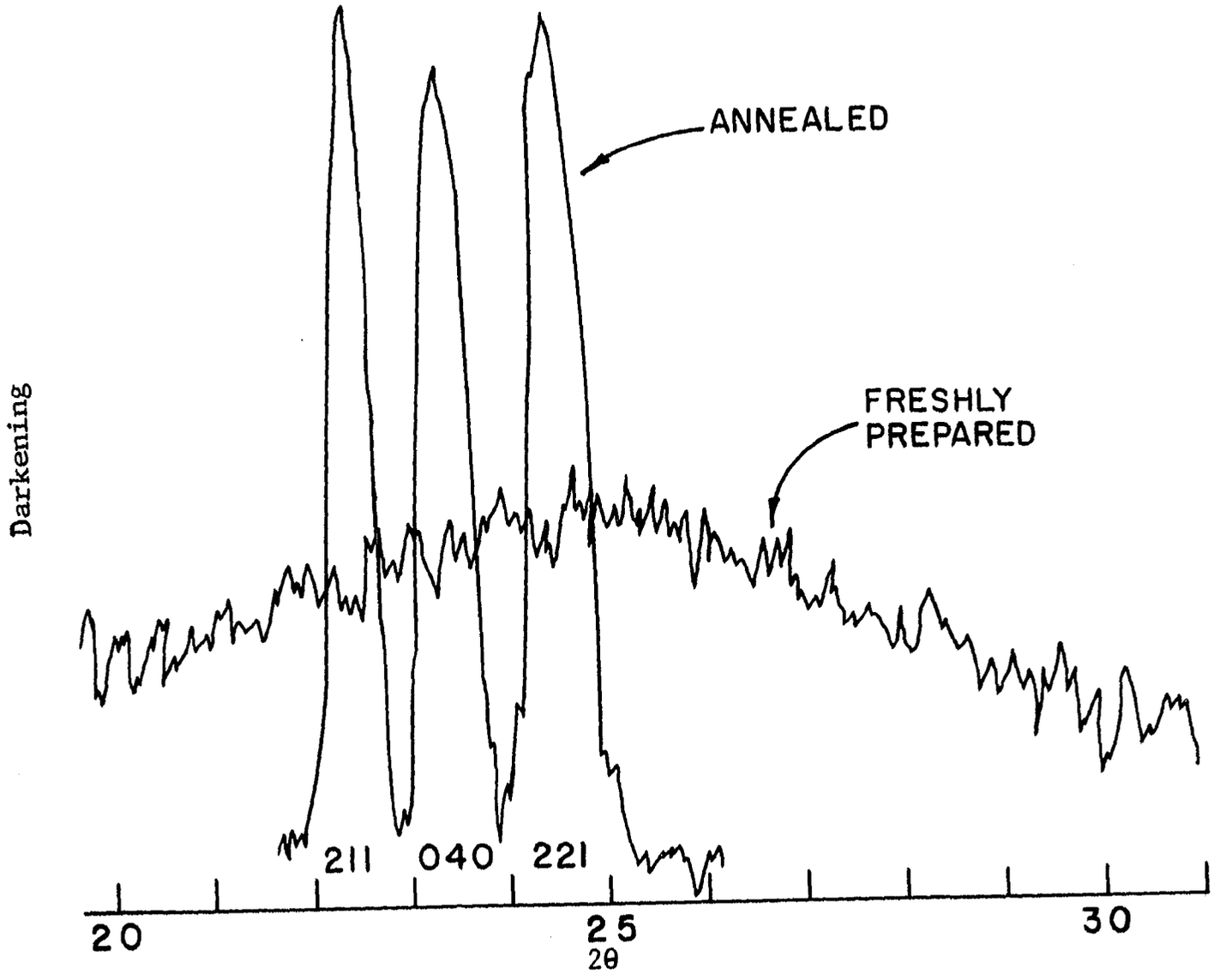

Figure 8. Densitometer tracings of the broad band and sharp-lined diffraction photographs of white rhenium oxide

teristic peroxide reaction or dissociation pressure discredit the Re_2O_8 description. The chemical analyses do substantiate a rhenium heptoxide stoichiometry, however, and the infrared spectra of the white and yellow oxides are essentially in agreement. Furthermore, the white material converts to yellow Re_2O_7 in the absence of potential reactants and without generating detectible products.

As produced, the dispersed oxide behaves similar to certain condensation aerosols, in particular some smokes (64,65). Although the particles displayed in Figure 7 were photographed after the smoke had deposited by sedimentation, many of the smaller particles still have the size of smoke particles (usually 5μ or less). Considering that sedimentation is usually accompanied by agglomeration of small particles, it is probable that the deposited particles are larger than the original particles in the dispersed state.

The apparent stability exhibited when the heptoxide smoke was bubbled through aqueous solutions has also been observed for other smokes such as ZnO, SO_3, and P_2O_5 (64). An adsorbed gas film on the smoke particles is one explanation given to explain the stability (64), but it appears that neither a stabilizing effect nor the presence of an adsorbed

layer have been verified experimentally (65). Remy (66), however, proposed that the apparent stability arises because most of the smoke particles never come into contact with the solution due to their small amplitudes of Brownian motion. It appears the correct explanation has not yet been identified.

The approximate crystallite size of the rhenium oxide smoke (calculated at about 20Å) might be indicative of the primary structural unit in the smoke. Other investigators (67, 68) have studied some oxide smokes[1] and identified the crystal structures of the smoke crystallites with the crystal structures observed for large crystals of the same material. In some cases, electron microscope studies showed regularly shaped crystallites linked together into the smoke structure. The sizes of the crystallites were generally larger (25Å-1000Å) than the calculated average size of the rhenium oxide crystallites; but the relatively smaller size of rhenium oxide might result because the complex bonding arrangements in crystalline Re_2O_7 (see Figure 4) could inhibit ordered crystallite growth during condensation.

---

[1]The studied smokes had structures that were generally cubic or hexagonal with relatively small lattice constants.

THE STRUCTURE OF THE MESOPERRHENATE ION

In 1933 the Noddacks (69) reported the formation of barium mesoperrhenate, $Ba_3(ReO_5)_2$, when barium perrhenate was fused with sodium hydroxide at red heat. The yellow mesoperrhenate crystals were stable in dry air but decomposed in water to form barium perrhenate and barium hydroxide. The Noddacks described barium mesoperrhenate as the barium salt of mesoperrhenic acid which they formulated as H_3ReO_5.

Also in 1933 Scharnow (70) reported the formation of a yellow mesoperrhenate compound upon evaporation of aqueous solutions of $Ba(ReO_4)_2$ and a large excess of $Ba(OH)_2$. The yellow compound deposited along with $Ba(OH)_2$ during evaporation and was subsequently purified by washing with alcohol. Chemical analyses performed on purified precipitates indicated an average barium to rhenium atom ratio of approximately 3.3 to 2, but Scharnow designated the yellow compound as $Ba_3Re_2O_{10}$ and suggested the extra barium content resulted from incomplete purification.

Further mesoperrhenate studies were not reported until the late 1950's and early 1960's when Scholder and others (71, 72,73) described the preparation and the chemical and X-ray characterization of a number of alkali and alkaline earth

metal penta- and hexa-oxorhenates(VII). The salts β-$Ba_3(ReO_5)_2$, α-$Ba_3(ReO_5)_2$, and $Ba_5(ReO_6)_2$ were reported for the barium cation. β-$Ba_3(ReO_5)_2$ is a low temperature modification of barium mesoperrhenate. The compound was synthesized by a reaction of $Ba(ReO_4)_2$ with either $BaCO_3$, BaO, or $Ba(OH)_2$ in oxygen at between 600°C and 800°C. Above 800°C the low temperature modification changes to the high temperature form of barium mesoperrhenate, α-$Ba_3(ReO_5)_2$. Barium orthoperrhenate, $Ba_5(ReO_6)_2$, is a red-orange compound that was described as isotypic with $Ba_5(IO_6)_2$. The chemical compositions of these compounds were determined by chemical analysis, and the different crystal structures were identified by X-ray powder diffraction techniques. None of the X-ray patterns were indexed or analyzed, however, and little is known about the crystal systems of the salts, the coordination of rhenium, or the rhenium-oxygen bond distances.

Even though detailed investigations of the mesoperrhenate ion have not been reported, some investigators have speculated about the geometry and the chemical nature of the ion. The Noddacks wrote the mesoperrhenate ion as ReO_5^{-3} (69), but Scharnow wrote it as $Re_2O_{10}^{-6}$ (70) without explaining his use of the dimeric formulation. Carrington and Symons (74) were

interested in the species in aqueous alkaline solution, and they formulated the reaction of perrhenate ion in concentrated alkali as

$$ReO_4^- + 2OH^- = ReO_4(OH)_2^{-3} = ReO_5^{-3} + H_2O \ .$$

They also presented evidence for an analogous ruthenium ion, $RuO_4(OH)_2^{-2}$, and they noted that $K_2OsO_4(OH)_2$ had been isolated from an aqueous alkaline solution of OsO_4.

The proposed $ReO_4(OH)_2^{-3}$ ion would require a rhenium coordination number of six. Evidence that rhenium(VII) exhibits six coordination with oxygen was first given by Sleight and Ward (75) who determined the crystal structures of $Ba(Li_{.5}Re_{.5})O_3$ and $Ba(Na_{.5}Re_{.5})O_3$. These compounds have ordered perovskite-type crystal structures with rhenium in six-fold coordination with the oxygens. The crystal structure of Re_2O_7 also exhibits a form of six-fold rhenium-oxygen coordination (see Figure 4).

Peacock (57) assumed that rhenium showed six coordination in the mesoperrhenate ion, and he suggested the ion was the dimeric species $Re_2O_{10}^{-6}$. He viewed the dimer as a dehydration product of $ReO_4(OH)_2^{-3}$.

Since many questions are unanswered about the nature of the mesoperrhenate ion, a knowledge of the geometrical struc-

ture of the ion is of interest in order to accurately describe the ion and know more about the coordination chemistry of rhenium(VII). At least three regular stereochemical forms are possible for an ion of empirical formula ReO_5^{-3}. A monomeric form may have either tetragonal pyramidal (C_{4v}) or trigonal bipyramidal (D_{3h}) symmetry, and a regular dimeric form can be described as two ReO_6 octahedral units sharing a common edge. An octahedral $ReO_4(OH)_2^{-3}$ ion is also a possible description for mesoperrhenates obtained from aqueous solutions, but this description is unlikely for mesoperrhenates prepared by the high temperature dry reaction between barium perrhenate and barium carbonate.

Experimental Procedure

Crystal preparation

Yellow compounds containing barium mesoperrhenate were prepared by two methods. The method of Scholder (73) was used to prepare β-$Ba_3(ReO_5)_2$ at 650°C and α-$Ba_3(ReO_5)_2$ at 900°C according to the reaction

$$Ba(ReO_4)_2 + 2BaCO_3 \overset{O_2}{=} Ba_3(ReO_5)_2 + 2CO_2.$$

The solution evaporation method of Scharnow (70) was employed to grow mixed mesoperrhenate crystals according to the following reaction which is written in agreement with the findings

of this present investigation

$$Ba(ReO_4)_2 + 7/3Ba(OH)_2 \overset{H_2O}{=} Ba_3(ReO_5)_2 \cdot 1/3Ba(OH)_2 + 2H_2O.$$

Beta barium mesoperrhenate formed as a very fine powder, but individual crystals were not distinguishable under an optical microscope, and single crystal X-ray techniques could not be applied. Alpha barium mesoperrhenate formed as small hexagonal platelets, but preliminary X-ray studies of numerous crystals always indicated imperfect material. The nature of the imperfection(s) is not apparent, and attempts to improve the quality by annealing were unsuccessful. Further investigations of this material have been described in Appendix B. Crystals synthesized using a modification of Scharnow's procedure were suitable for single crystal X-ray study, however, as eventually discovered in this investigation, the material was not barium mesoperrhenate but a mixed salt of barium mesoperrhenate and barium hydroxide, $Ba_3(ReO_5)_2 \cdot 1/3Ba(OH)_2$. It is interesting to note that the calculated barium to rhenium atom ratio for this compound is 3.3 to 2, which agrees favorably with Scharnow's original analyses.

The apparatus used for the preparation of $Ba_3(ReO_5)_2 \cdot 1/3Ba(OH)_2$ is diagrammed in Figure 9. The reaction container, B, was fabricated from a 30 mm sealing tube containing a

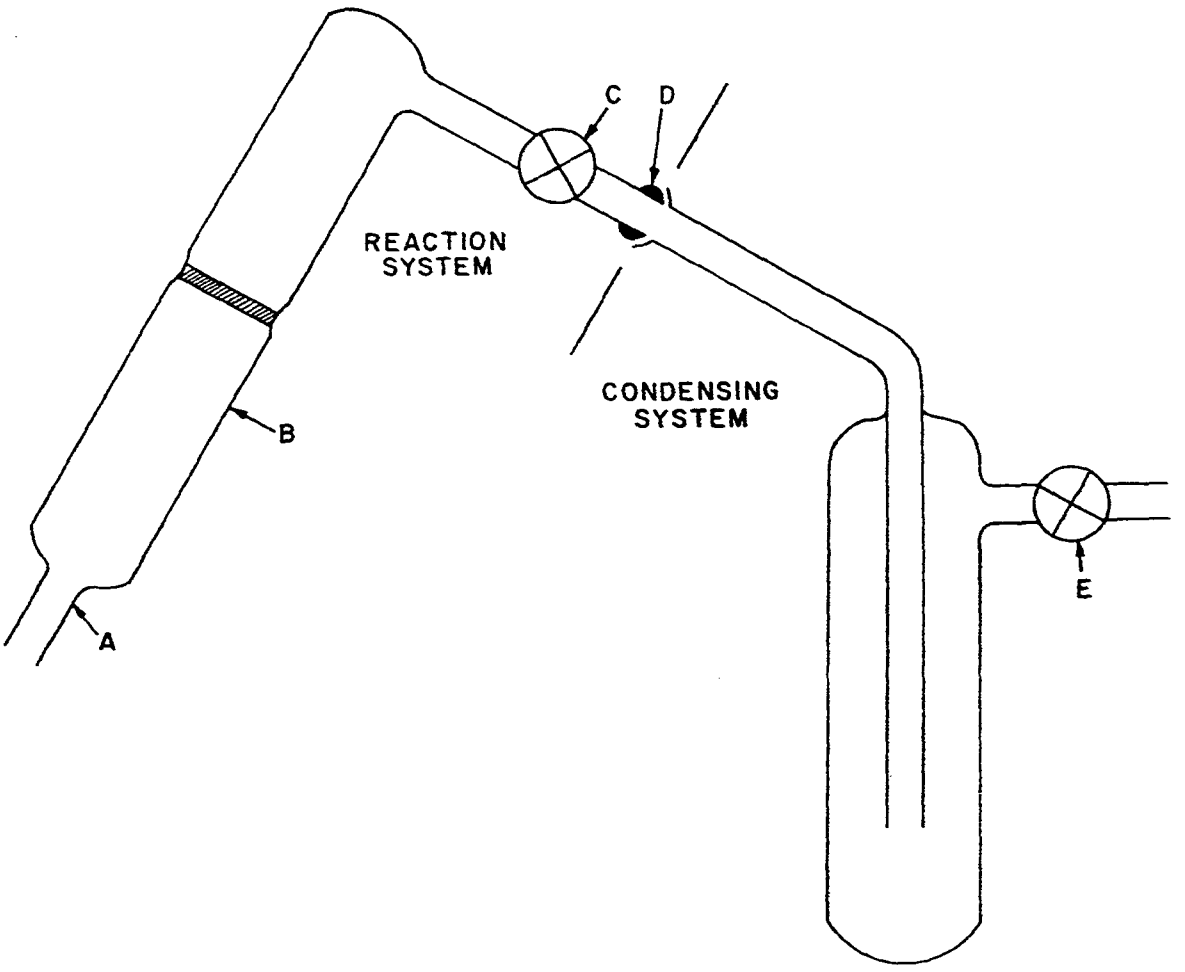

Figure 9. A representation of the apparatus used to prepare $Ba_3(ReO_5)_2 \cdot 1/3\ Ba(OH)_2$

medium size porous glass disc. The disc was employed to cut down on solution bumping and subsequent splashing onto the container walls. Splashing usually resulted in a very crusty precipitate and poorly developed crystals. In a typical preparation, 1 g $Ba(ReO_4)_2$[1] and 4 g $Ba(OH)_2 \cdot 8H_2O$ were introduced into the reaction container through an entrance tube, A. The tube was sealed shut, and the entire reaction container was evacuated through stopcock C. About 50 ml of water, freshly distilled from a NaOH solution in a CO_2-free system, was drawn into the reaction container through stopcock C. The pressure in the container was made slightly in excess of atmospheric pressure by filling with nitrogen, and after flushing the condensing system to remove possible CO_2, the reaction system and the condensing system were joined at D. The pressures of the two systems were equilibrated by opening stopcock C while stopcock E was kept closed. The bottom half of the reaction container was placed in a boiling water bath, and after the $Ba(ReO_4)_2$-$Ba(OH)_2$ solution had reached the temperature of the water bath, stopcock E was opened and the pressure within the whole apparatus decreased

---

[1] $Ba(ReO_4)_2$ was prepared by neutralization of $HReO_4$ with $Ba(OH)_2$. $HReO_4$ was prepared from Re_2O_7 and H_2O.

to atmospheric pressure. Stopcock E was closed to isolate the system from the atmosphere, and the solution in the reaction container was slowly evaporated to dryness.

When evaporation was completed, the reaction bulb was opened and the $Ba_3(ReO_5)_2 \cdot 1/3Ba(OH)_2$ crystals were scraped from the walls along with $Ba(OH)_2$. The mixture was washed with absolute methanol to remove $Ba(OH)_2$, and the purified precipitate was dried at 120°C for one hour. The yellow mesoperrhenate crystals grown by this procedure were easily recognized as hexagonal columns which could be conveniently aligned along the c axis for X-ray investigation.

Preliminary crystal data

Single crystals of $Ba_3(ReO_5)_2 \cdot 1/3Ba(OH)_2$ were examined by precession and Weissenberg film techniques and assigned to the hexagonal crystal system. The Laue symmetry is $P_{6/mmm}$ and the only observed systematic extinctions were $hh\bar{0}l$ reflections for l being odd. This indicated the possible space groups: $P_{6_3/mcm}$, P_{6_3cm}, $P\bar{6}c2$.

A single crystal was mounted with Duco cement on the tip of a glass fiber with the crystallographic c axis aligned approximately along the fiber axis. The lattice constants and their estimated standard deviations were obtained from a

least-squares refinement (76) of 23 independent reflection angles observed at room temperature in the back reflection region ($100^{o} \leq 2\theta \leq 165^{o}$) using a General Electric single-crystal orienter and CrK_{α} radiation [$\lambda(K_{\alpha_1}) = 2.28962\text{Å}$ and $\lambda(K\bar{\alpha}) = 2.29092\text{Å}$]. The Nelson-Riley extrapolation function was used, and the measured cell parameters and their estimated standard deviations are $a = 10.9374 \pm .0025\text{Å}$, $c = 7.8436 \pm .0031\text{Å}$, $V = 812.6\text{Å}^3$. The observed density was 5.94 g/cm^3 (by displacement), and the calculated density for three units of $Ba_3(ReO_5)_2 \cdot 1/3Ba(OH)_2$ per unit cell is 6.14 g/cm^3.

The dimensions of the hexagonal crystal used for the cell parameter measurements and the crystal structure determination were in succession 0.0127 x 0.0113 x 0.0079 x 0.0108 x 0.0128 x 0.0061 mm for the six sides and 0.0504 mm high. The dimensions were measured from photomicrographs taken with plane polarized light on a Bausch and Lomb metallograph and scaled to similar pictures of a standard ruled grating.

X-ray Intensity Data

Three-dimensional intensity data up to 75^{o} in 2θ were measured with molybdenum K_{α} radiation at room temperature for one half of the first octant of reciprocal space. A General Electric XRD-5 X-ray unit, equipped with a single-crystal

orienter, a pulse height analyzer (4.5-15V), a strip chart recorder, and a scintillation counter was used in conjunction with the moving-crystal-moving-counter measurement procedure (θ-2θ coupling), a 3° take-off angle, and a 1.6° diffraction beam aperture. A zirconium foil, placed in the diffracted beam path, reduced the intensity of undesired molybdenum K_{β} radiation to less than two percent of the K_{α} intensity. A 200 sec. scan through 3.33° in 2θ was made for each reflection to determine the integrated intensity, and this was followed by a similar background scan with an omega offset of 2° (77). The integrated intensities and the corresponding backgrounds of the 300 and 004 reflections were measured repeatedly during the collection of data in order to monitor the stability of the crystal in the X-ray beam. The net intensities of these two reflections remained constant to within $\pm$ 3%. These fluctuations were interpreted as drift in the electronic measurement apparatus and no decomposition corrections were applied. Corrections for possible nonlinearity of the counting system were also found to be unnecessary.

Diffracted beam intensities were rather low because of the high absorption effects (μ = 358.6 cm^{-1} for Mo K_{α}) and the small crystal size. Individual reflections were consid-

ered observed if the net intensity satisfied two requirements. First, the net intensity, I_{net}, had to be at least three times greater than the uncertainty in the measurement, $\sigma(I_{net})$. I_{net} and $\sigma(I_{net})$ were calculated according to the relationships

$$I_{net} = I_{hk\ell} - I_{bkg}$$

$$\sigma(I_{net}) = (I_{hk\ell} + I_{bkg})^{\frac{1}{2}}$$

where $I_{hk\ell}$ is the measured integrated peak intensity and I_{bkg} is the measured background intensity. Second, a distinguishable diffraction peak had to be traced out by the strip chart recorder. A total of 808 reflections were measured and 397 were judged observed. Those reflections judged unobserved were not included in the least-squares refinements.

The measured integrated peak intensity for each reflection was corrected for measured background intensity, Lorentz-polarization effects (Lp), absorption effects (1/T), and streak intensity (I_{stk}). No extinction corrections were applied. The magnitude of the relative structure factors, $|F_{hk\ell}|$, was calculated for all reflections according to Equation 2 below. If the corrected peak intensity was negative, the structure factor was set equal to zero.

$$|F_{hk\ell}| = \left[\frac{1}{T}\left(\frac{I_{hk\ell} - I_{bkg}}{Lp} - I_{stk}\right)\right]^{\frac{1}{2}} \qquad (2)$$

The Lorentz-polarization correction was made according to Equation 3 where $\theta_{hk\ell}$ represents the Bragg angle for the hkℓ reflection.

$$Lp = \frac{1 + \cos^2 2\theta_{hk\ell}}{2\sin 2\theta_{hk\ell}} \qquad (3)$$

The Lorentz factor depends on the geometry of the measurement device and corrects the measured intensities for the different time intervals that given sets of crystal planes are in position to diffract. The polarization factor corrects for polarization of the diffracted X-ray beam.

The intensities of all reflections were corrected for X-ray absorption effects. A program to calculate X-ray transmission factors (T) had been written by Busing and Levy (78) and was modified for an IBM 360 computer by Dr. J. V. Ugro. This program required the crystal dimensions, the orientation of the crystal, and the linear absorption coefficient. The calculated transmission factors ranged between 0.55 and 0.61.

Streak corrections were made using a modification (79) of the method of Williams and Rundle (80). Streaking results from noncharacteristic X-ray radiation diffracting at the same angle as characteristic radiation. For example, if diffraction takes place for a 400 reflection at the characteristic wavelength λ, then diffraction also takes place for the 300 reflection, but

at wavelength 4/3 λ. Likewise, diffraction for the 200 reflection occurs at 4/2 λ, and so on for all h00 reflections. Since the intensities of wavelengths shorter than λK_α were sufficiently reduced by the zirconium filter, and the intensities of wavelengths longer than $2\lambda_{K\alpha}$ were very low, streak corrections were only necessary over the wavelength range $\lambda_{K\alpha} < \lambda < 2\lambda_{K\alpha}$.

Streaking is also a function of the mosaic nature of a crystal as well as the intensity distribution of the X-ray source, therefore, the streak intensity distribution must be determined experimentally for each crystal. In this structure determination, the streak intensity distributions of four prime reflections (502, 304, 421, 115) were measured as a function of wavelength. The measured streak intensities were corrected for background and the Lorentz-polarization effect, normalized to a common scale, averaged, and tabulated as streak intensity versus wavelength. The net integrated intensity due to characteristic X-ray radiation was then obtained by subtracting the streak contributions of noncharacteristic radiation from the measured intensity. The streak intensity correction exceeded 3 percent of the uncorrected intensity for only 48 of the observed reflections. The functional form of the streak

intensity correction and the functional forms of other equations used during the solution of the structure have been presented in Appendix C.

In order to weight the observed structure factors ($w = 1/\sigma^2(F_{hk\ell})$) during the least-squares refinements, the variance of each structure factor was calculated for the observed reflections according to the equation

$$\sigma^2(F_{hk\ell}) = \sum_{X_i} \left(\frac{\partial F_{hk\ell}}{\partial X_i}\right)^2 \sigma^2(X_i) \qquad (4)$$

where $F_{hk\ell}$ is calculated from Equation 2 above, and the variables X_i include $I_{hk\ell}$, I_{bkg}, I_{stk}, and T. The variance of the quantities $I_{hk\ell}$, I_{bkg}, and T were assigned as follows:

$$\sigma^2(I_{hk\ell}) = I_{hk\ell} + (K_1\ I_{hk\ell})^2$$
$$\sigma^2(I_{bkg}) = I_{bkg} + (K_1\ I_{bkg})^2$$
$$\sigma^2(T) = (K_2\ T)^2.$$

K_1 was assigned the value 0.03 corresponding to the fluctuations observed in the intensities of the 300 and 004 monitored reflections. K_2 was assigned the value 0.03 as an estimate of the precision of the calculated transmission factors. The variance of the streak intensity was calculated by application of a generalized form of Equation 4 to the appropriate streak

equation (see Appendix C).

Solution of the Crystal Structure

A computer program for calculating an unsharpened three-dimensional Patterson function in the hexagonal crystal system was written (see Appendix C), and a Patterson map was calculated using the relative structure factor data from all measured reflections. An examination of the 0,0,w Harker section of the Patterson map was made to distinguish between the three possible space groups deduced from the observed Laue symmetry and the systematic extinction conditions. The space groups $P\bar{6}c2$ and $P_{63/mcm}$ have symmetry related positions that could lead to 0,0,w Patterson peaks at 0,0,2z and 0,0,$\frac{1}{2}$-2z in addition to 0,0,$\frac{1}{2}$. A crystal structure in the space group P_{63cm}, however, could only have symmetry related 0,0,w peaks at 0,0,$\frac{1}{2}$. Since the 0,0,w Harker section of the calculated Patterson map contained a significant peak at only 0,0,$\frac{1}{2}$, the P_{63cm} space group (No. 185 (81)) was used for subsequent calculations and refinements of the $Ba_3(ReO_5)_2 \cdot 1/3Ba(OH)_2$ crystal structure.

Trial coordinates for one rhenium and two barium atoms were determined by interpretation of the Patterson map. Using the full-matrix least-squares computer program, ORFLS (82), a refinement was performed on these atom coordinates and an

over-all temperature factor. Structure factors calculated during this refinement gave an unweighted discrepancy factor, R, of 0.084 and a weighted discrepancy factor, R', of 0.097 where these factors are defined in Equation 5 and Equation 6 below.

$$R = \frac{\sum |F_o - F_c|}{\sum |F_o|} \tag{5}$$

$$R' = \frac{(\sum w(F_o - F_c)^2)^{\frac{1}{2}}}{(\sum w F_o^2)^{\frac{1}{2}}} \tag{6}$$

w is the weighting factor defined previously as $1/\sigma^2(F_{hk\ell})$, and F_o and F_c represent the observed and calculated structure factors. The weighted discrepancy factor, R', was the quantity minimized by ORFLS. The atomic scattering factors (neutral atoms) used for the structure factor calculations were obtained from the compilation by Hanson and others (83).

When individual isotropic temperature factors were introduced for the rhenium and barium atoms and a further least-squares refinement was performed, the R factor dropped to 0.080 and R' dropped to 0.094.

Since the agreement between the heavy atom trial structure and the observed structure appeared quite good, a computer program was written to calculate a three dimensional Fourier electron density difference map (see Appendix C). Difference

maps are commonly employed as an aid to indicate how a trial structure compares to the structure under investigation. When a trial structure is sufficiently close to describing the measured structure, an electron density difference map might indicate positions (peaks) where atoms exist in the measured structure but have not been placed in the trial structure. Likewise, a difference map might indicate positions (depressions) where atoms placed in the trial structure do not correspond to atoms in the measured structure. The proper interpretation of peaks and depressions in an electron density difference map, therefore, can be very beneficial to the solution of a crystal structure.

In order to locate trial positional parameters for oxygen atoms, a difference map was computed for the heavy atom trial structure using individual isotropic temperature factors. Since the space group $P6_3cm$ is acentric, phase angles were computed from the real and imaginary parts of the structure factors calculated by ORFLS, and values of $|F_o| - |F_c|$ were used as the Fourier coefficients. In addition to the structure factors for the measured reflections, the Fourier calculation required structure factors for $\bar{h}k\ell$ reflections which had not been measured directly. Values for these structure factors

were generated from the structure factors of measured hkℓ reflections by employing appropriate symmetry relationships and assuming Friedel's Law.

Examination of the calculated difference map revealed five peaks (three independent atom positions) at chemically reasonable bonding distances from the location of each rhenium atom. Oxygen atoms were placed into the heavy atom trial structure at these positions, and after refinement of all positional parameters, anisotropic temperature factors for the heavy atoms, and isotropic temperature factors for the oxygen atoms, the R factor reduced to 0.054 and R' to 0.053.

Another electron density difference map was calculated to determine the location of the hydroxide ion. Since the hydrogen atom was not located from the difference synthesis, the hydroxide ion was placed into the structure as an oxygen atom. A final difference synthesis was calculated and showed a residual peak of 0.8 $e^-/\text{Å}^3$ at the origin.

With all atoms now placed into the trial structure, the barium and rhenium structure factors were corrected for the real and imaginary parts of anomalous dispersion (84). A final least-squares refinement on all positional parameters, anisotropic temperature factors for barium and rhenium atoms, and

isotropic temperature factors for oxygen atoms (including the hydroxide oxygen) gave values of R = 0.051 and R' = 0.050. The standard deviation for an observation of unit weight, defined as

$$\left(\frac{\sum w(|F_o| - |F_c|)^2}{n-m}\right)^{\frac{1}{2}},$$

was 1.001 where n is the number of observations -397- and m is the number of variables -28-. On the final least-squares cycle, the shift in each positional and thermal parameter was insignificant with respect to the estimated standard deviations of the respective parameters.

Since the determined structure belongs to an acentric space group and corrections were made for anomalous dispersion, a check was made on the absolute crystal configuration. A least-squares refinement was performed on a different trial structure where the atom positional parameters of the previously determined structure were transformed through a center of inversion, i.e., $\bar{x},\bar{y},\bar{z}$ was substituted for x,y,z for each atom. In this refinement the R factor increased to 0.054 and R' to 0.054. According to the significance tests proposed by Hamilton (85), the inverted trial structure can be rejected at the 0.005 significance level, and the crystal structure, as determined, has the correct absolute configuration.

The final atom positional parameters and the final atom thermal parameters are presented in Table 6 and Table 7 along with the standard deviations. A listing of the absolute values of the 397 observed structure factors (in electrons) and the corresponding calculated structure factors is given in Figure 10. A listing of the 411 unobserved structure factors (in electrons) and the corresponding calculated structure factors is given in Figure 11.

Discussion

A drawing of the unit cell of the $Ba_3(ReO_5)_2 \cdot 1/3\ Ba(OH)_2$ crystal structure is presented in Figure 12 where the boundaries of the cell and the $1\bar{1}0$ lattice plane have been outlined. The drawing was made with the plotting program ORTEP (86) with the atoms represented as 75 percent probability thermal ellipsoids. The cell contains three units of $Ba_3(ReO_5)_2 \cdot 1/3\ Ba(OH)_2$. The labeled Ba_2 atoms lie at the 2/3,1/3,0, 2/3,1/3,1/2, and 2/3,1/3,1 positions. The labeled Ba_1, Re, O_3, and OH^1 atoms lie in the front 010 lattice plane which is also a mirror plane in the P_{63cm} space group. The labeled O_1 and O_2 atoms lie within the boundaries of the outlined cell and are related to O_1' and O_2' by the 010 mirror plane. The unlabeled atoms

---

[1] OH^- was represented in the structure by an oxygen atom.

Table 6. Final positional parameters for $Ba_3(ReO_5)_2 \cdot 1/3\ Ba(OH)_2$

Atom	Wyckoff position	X[a]	Y[a]	Z[a]
Re	c	0.60936(15)	0.0[b]	0.29374(45)
Ba_1	c	0.26417(26)	0.0[b]	0.24166(58)
Ba_2	b	0.66667[b]	0.33333[b]	0.0[c]
O_1	d	0.7409(25)	0.1324(25)	0.4313(27)
O_2	d	0.5541(22)	0.1320(19)	0.2569(28)
O_3	c	0.7084(33)	0.0[b]	0.1277(43)
OH	a	0.0[b]	0.0[b]	0.267(18)

[a]Numbers in parentheses represent standard deviations occurring in the last digit of the parameter.

[b]These coordinates are fixed by symmetry.

[c]Space group P_{6_3cm} is polar in Z. This parameter was fixed at 0.0 as a point of reference.

Table 7. Final thermal parameters for $Ba_3(ReO_5)_2 \cdot 1/3\ Ba(OH)_2$[a]

Atom	Anisotropic thermal parameters ($\times 10^5$)[b]						Equivalent[c] isotropic factor, $Å^2$	Isotropic factor, $Å^2$
	B_{11}	B_{22}	B_{33}	B_{12}	B_{13}	B_{23}		
Re	275(11)	170(15)	317(16)	85(8)	46(20)	0[d]	0.83	--
Ba_1	396(20)	270(24)	519(32)	135(12)	16(27)	0[d]	1.27	--
Ba_2	266(15)	266(15)	289(31)	133(8)	0[d]	0[d]	0.87	--
O_1	--	--	--	--	--	--	--	1.58(35)
O_2	--	--	--	--	--	--	--	1.26(31)
O_3	--	--	--	--	--	--	--	1.73(60)
OH	--	--	--	--	--	--	--	7.10(1.60)

[a]Numbers in parentheses are standard deviations occurring in the last digit of the parameter.

[b]The form of the anisotropic temperature factor is $e^{-}(B_{11}h^2 + B_{22}k^2 + B_{33}\ell^2 + 2B_{12}hk + 2B_{13}h\ell + 2B_{23}k\ell)$.

[c]The isotropic temperature factor equivalent to the anisotropic form was calculated as $B_{isotropic} = 4/3(B_{11}a^2 + B_{22}a^2 + B_{33}c^2 + 2B_{12}a^2 \cos\gamma + 2B_{13}ac \cos\beta + 2B_{23}ac \cos\alpha)$, where the B's are the anisotropic thermal parameters and a, c, α, β, γ are the unit cell lattice parameters (87).

[d]These thermal parameters are fixed at zero by symmetry.

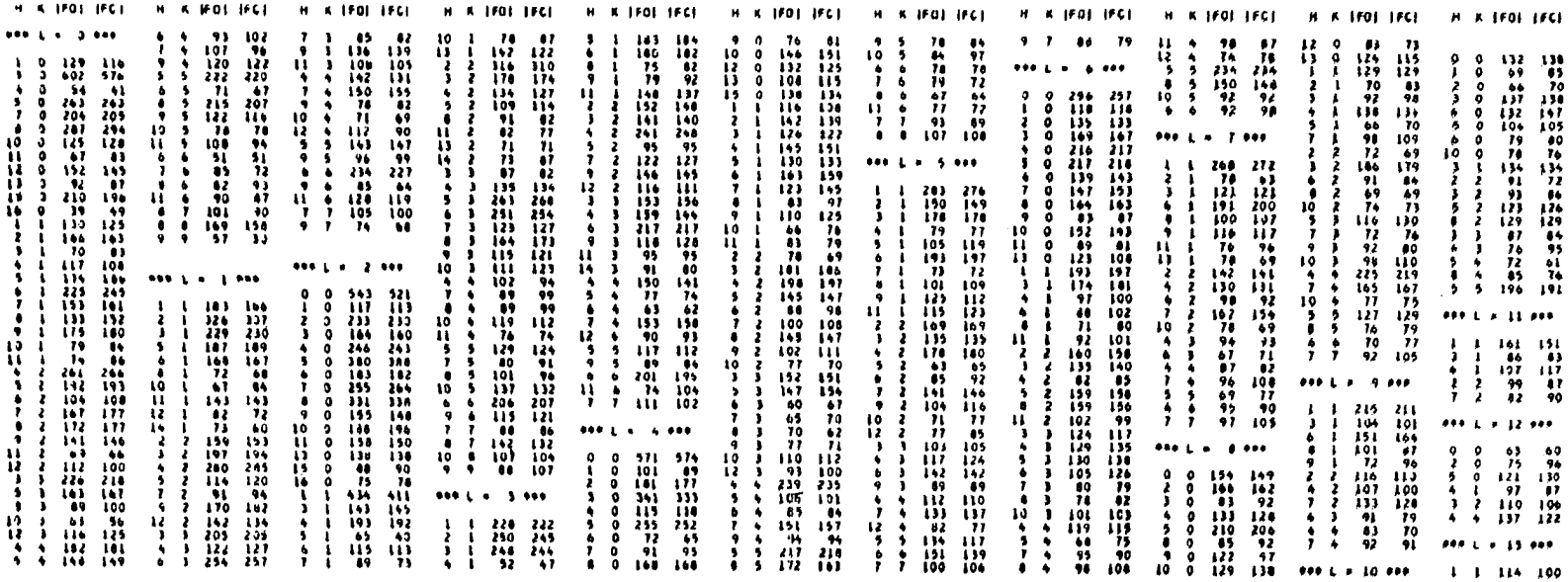

Figure 10. Observed and calculated structure factors (in electrons) for $Ba_3(ReO_5)_2 \cdot 1/3\ Ba(OH)_2$

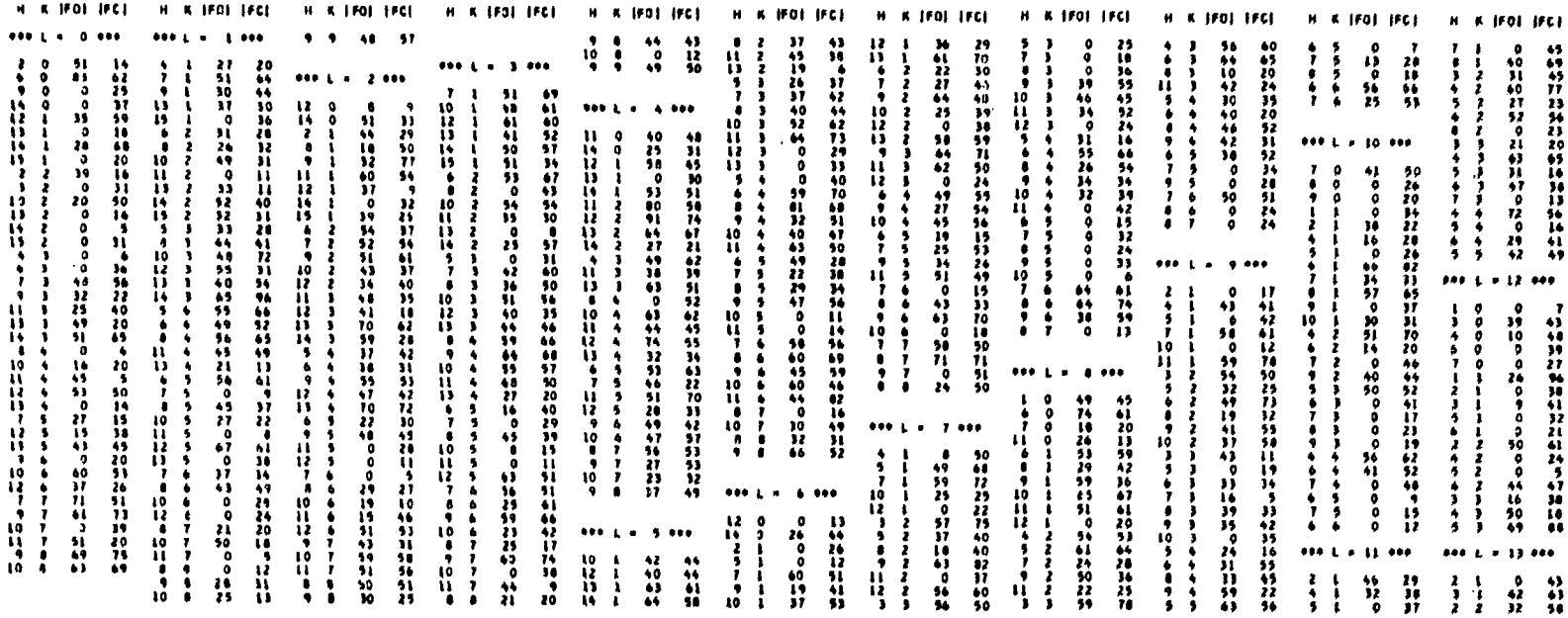

Figure 11. Unobserved and calculated structure factors (in electrons) for $Ba_3(ReO_5)\cdot 1/3\ Ba(OH)_2$

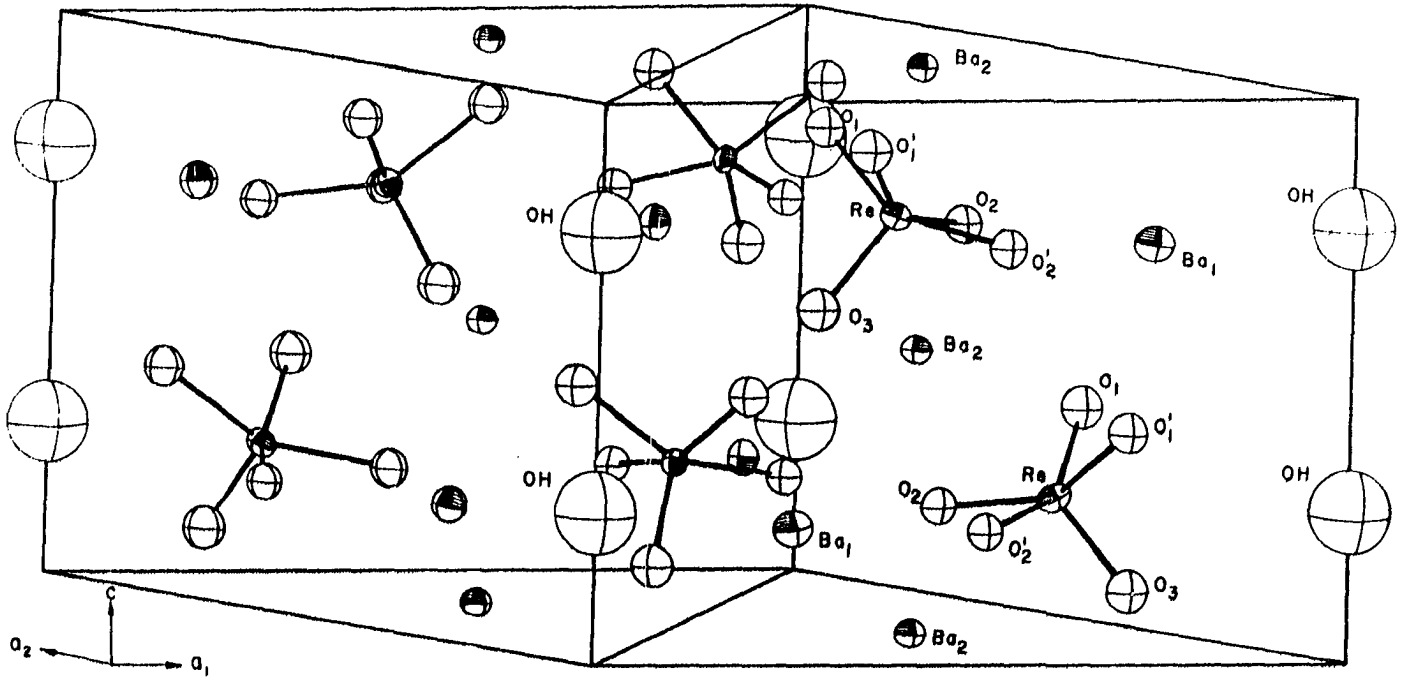

Figure 12. A drawing of the unit cell of $Ba_3(ReO_5)_2 \cdot 1/3\ Ba(OH)_2$

are related to the corresponding labeled atoms by appropriate symmetry operations, and in order to simplify this drawing, the atoms residing in or near the back 010 plane and the right 100 plane were not included (except for the OH's).

The crystal structure shows the existence of discrete monomeric mesoperrhenate ions (ReO_5^{-3}) with five oxygens arranged around each rhenium in the geometry of a tetragonal pyramid. The shortest rhenium-rhenium distances are 4.5926 $\pm$ .0023Å, and only the five oxygens are situated near enough to rhenium to be interpreted as being bonded to rhenium. Near the oxygens of the mesoperrhenate ions and around the oxygens of the hydroxide ions are the barium counter ions. The barium-oxygen near-neighbor distances and the standard deviations are presented in Table 8. The distances and standard deviations were calculated by the computer program ORFFE (88). The near-neighbor to Ba_2 distances are somewhat less than the near-neighbor distances to Ba_1, therefore it appears the crystal packing is largely determined by the Ba_2-near-neighbor interactions. In addition, the arrangement of near-neighbors around Ba_1 is quite irregular. The observed 2.70-2.78Å Ba_2-near-neighbor distance range is in agreement with common barium-oxygen distances; the sums of the Slater radii and the Pauling

ionic radii are both 2.75Å (89,90). The tighter packing around Ba_2 implies a stronger interaction between Ba_2 and its near-neighbors, and this would explain why the temperature factor of Ba_2 is smaller than the temperature factor of Ba_1 (see Table 7).

Table 8. A tabulation of barium to oxygen near-neighbor distances

Atoms	Number of occurrences	Near-neighbor[a] distance, Å
Ba_1-O_1	2	2.870(23)
Ba_1-O_1	2	2.819(21)
Ba_1-O_2	2	2.753(20)
Ba_1-O_3	1	3.043(32)
Ba_1-O_3	2	3.179(22)
Ba_1-OH	1	2.897(10)
Ba_2-O_1	3	2.750(22)
Ba_2-O_2	3	2.700(20)
Ba_2-O_2	3	2.778(19)

[a]Numbers in parentheses are the standard deviations occurring in the last digit of the near-neighbor distance.

The main interest in the crystal structure of $Ba_3(ReO_5)_2 \cdot 1/3\ Ba(OH)_2$ is in the identity of the mesoperrhenate ion. A drawing (87) of the ion is presented in Figure 13 and the

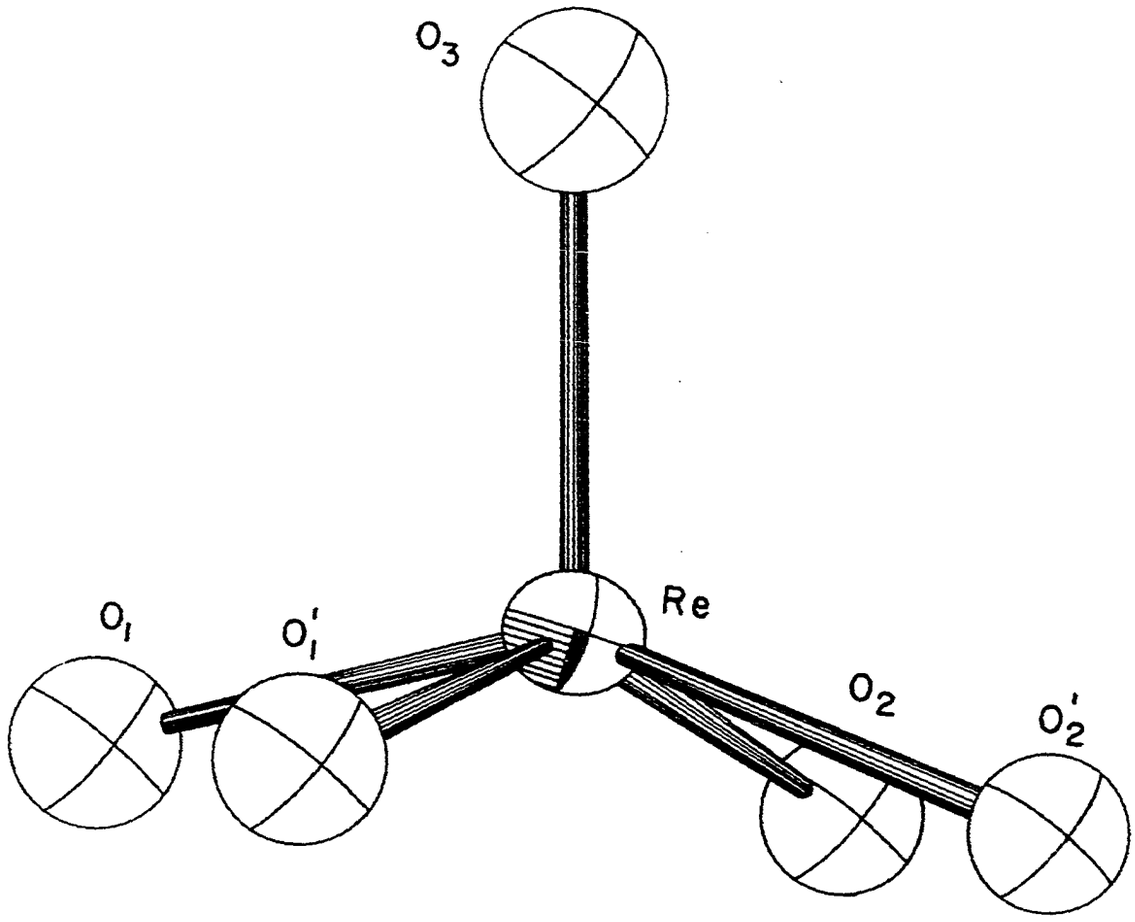

Figure 13. A drawing of the mesoperrhenate ion, ReO_5^{-3}

dimensions of the ion are given in Table 9. Re and O_3 lie in a mirror plane of symmetry, and in Figure 13 the mirror relates the primed basal oxygen atoms to the corresponding unprimed atoms. The basal oxygen atoms (O_1-O_2-O_2'-O_1') are arranged as a square plane with measured angles of 90.10° and 89.90°. The basal oxygen-oxygen separations are equal within experimental uncertainties and show an average value of 2.49Å. This compares with 2.80Å for twice the Pauling ionic radius of $O^=$ (90). The Re-O_1 and Re-O_2 bond distances are 1.802 ± .022Å and 1.845 ± .019Å respectively, and although they are essentially independent bond lengths, the hypothesis that the bond lengths are equal is acceptable at the 0.14 significance level; therefore according to accepted criteria (91,92), an average rhenium to basal oxygen bond distance of 1.82Å is applicable. Hence, the bonds can be regarded as equivalent. The rhenium, however, is not bonded in the plane of the basal oxygens but sits 0.50Å above the plane. This displacement is probably assumed to reduce electrostatic repulsions between the apex and basal oxygens.

The bond length of 1.69Å between rhenium and O_3, the apex oxygen, is significantly different and shorter than the bond length between rhenium and the basal oxygens (1.82Å).

Table 9. Dimensions of the mesoperrhenate ion

Atoms	Distance, Å[a]	Angle, deg.[a]
Re-O_1	1.802(22)	
Re-O_2	1.845(19)	
Re-O_3	1.693(33)	
O_1-O_1'	2.509(45)	
O_1-O_2	2.457(30)	
O_1-O_2'	3.509(30)	
O_1-O_3	2.716(33)	
O_2-O_2'	2.500(35)	
O_2-O_3	2.897(37)	
Re-O_{plane}	.499	
O_1-Re-O_1'		88.21(140)
O_1-Re-O_2		84.67(93)
O_2-Re-O_2'		85.30(119)
O_1-Re-O_2'		148.24(95)
O_1-Re-O_3		101.93(109)
O_2-Re-O_3		109.83(104)
O_1-O_2-O_2'		90.10(66)
O_2-O_1-O_1'		89.90(66)

[a]Numbers in parentheses are the standard deviations occurring in the last digit.

Both distances are shorter than the sum of the Slater radii (1.95Å), and this difference is attributed to multiple bond character[1]. Since the apex bond is shortest, it would presumably show the highest bond order. It should also be noted that the interactions of O_3 with the barium cations are probably weak. The shortest barium-O_3 distances are 3.04Å and 3.18Å which are considerably more than the 2.70Å and 2.75Å shortest distances for O_2 and O_1.

The angles between the apex oxygen, rhenium, and the basal oxygens are different by 8°; angle O_1-Re-O_3 is 102° and angle O_2-Re-O_3 is 110°[2]. Since the difference exceeds the experimental uncertainty, the geometry of ReO_5^{-3} in the crystal must be described as a tetragonal pyramidal ion which is slightly distorted by the sideways displacement of the apex oxygen. In the absence of distortion, however, ReO_5^{-3} would have C_{4v} symmetry.

---

[1]A possible interpretation of bonding is to assume that the 6s, 6p, and 5d rhenium orbitals hybridize to form $sp^3d_{x^2-y^2}$ sigma bonding hybrid orbitals. The d_{xy}, d_{xz}, and d_{yz} orbitals are then available for π bonding.

[2]Gillespie (93) calculated this angle for an electrostatic model where five electron pairs reside on the surface of a sphere and undergo mutual repulsion according to an r^{-n} law. For the square-pyramidal configuration, as $n \to \infty$, the four basal electron pairs reside on the equator, but for $n < \infty$ the electron pairs drop below the equator. For n = 8-12, the calculated angle is about 100°.

It is difficult to compare ReO_5^{-3} to other Re(VII) structures since the mesoperrhenate ion appears to be the only reported case of five coordinate Re(VII). However, a comparison of the rhenium-oxygen bond distances with four coordinate Re(VII) shows fairly good agreement. The rhenium-oxygen distance in gaseous ReO_3Cl is $1.761 \pm .003$Å (94) and in $KReO_4$ is $1.77 \pm .03$Å (95). The distances in Re_2O_7, which shows tetrahedral and pseudo-octahedral coordination (see Figure 4), range from 1.66Å to 2.16Å.

Other Mesoperrhenate Studies

U.V.-visible spectra

The reflectance spectra of the yellow compounds α-$Ba_3(ReO_5)_2$, β-$Ba_3(ReO_5)_2$, and $Ba_3(ReO_5)_2 \cdot 1/3\ Ba(OH)_2$ were obtained on a Beckman DU spectrophotometer equipped with a diffuse reflectance attachment. The spectra were measured at intervals from 10 to 25 millimicrons in the 320 to 650 millimicron region, and barium carbonate was used as a reflectance standard. The spectra of all three compounds consisted of a continuous absorption band beginning at about 450-500 millimicrons and extending into the ultraviolet region. This spectrum is illustrated in Figure 14 and labeled C. The spectra of the perrhenate ion in aqueous solution and presum-

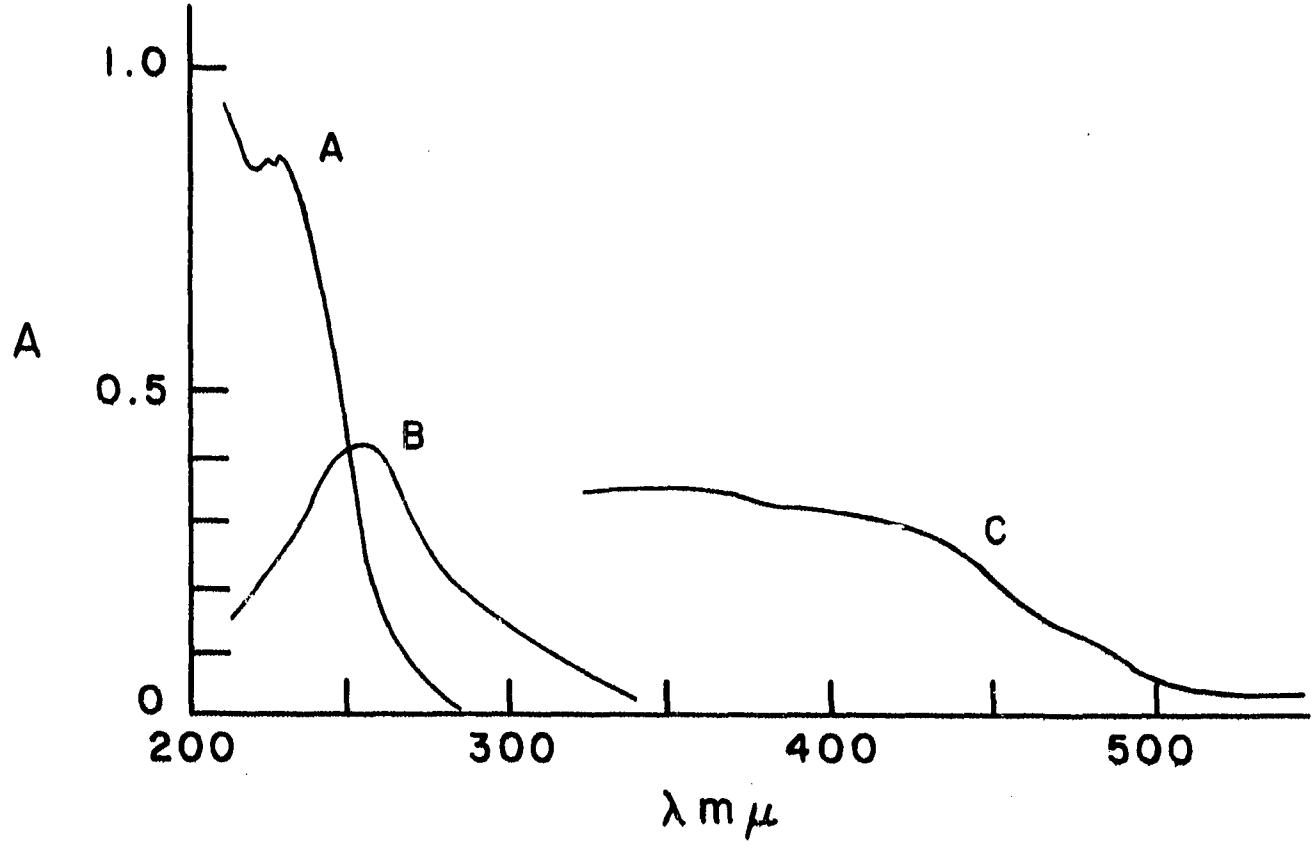

Figure 14. U.V.-visible spectra of mesoperrhenate and perrhenate species
A. 2.3×10^{-4} M $KReO_4$
B. 2.2×10^{-4} M $KReO_4$ in ~ 15 M NaOH
C. Reflectance spectrum: α-$Ba_3(ReO_5)_2$, β-$Ba_3(ReO_5)_2$, $Ba_3(ReO_5)_2 \cdot 1/3\ Ba(OH)_2$

ably the free mesoperrhenate ion (96)[1] (an alkaline perrhenate solution) have also been illustrated in Figure 14 as A and B respectively.

Since the spectrum exhibited by the solid mesoperrhenates (C) and the solution spectrum of the free mesoperrhenate ion (B) do not show substantial agreement, it is very probable that the tetragonal pyramidal ReO_5^{-3} ion has a different configuration in solution and possibly does not exist as the same chemical species. The solution ion is likely to be a more solvated species, perhaps the $ReO_4(OH)_2^{-3}$ ion proposed by Carrington and Symons (74).

Infrared spectra

The near infrared spectra of α-$Ba_3(ReO_5)_2$ and $Ba_3(ReO_5)_2 \cdot 1/3\ Ba(OH)_2$ were recorded with a Beckman IR-7 spectrophotometer. The solids were prepared in Nujol and placed between cesium iodide windows for spectral measurements. The observed spectra are presented in Figure 15. The peaks marked by an X are due to Nujol. The α-$Ba_3(ReO_5)_2$ spectrum shows absorption peaks at 975 cm^{-1} (narrow), 917 cm^{-1}, and

---

[1]The solution spectrum (B) attributed to the mesoperrhenate ion is of a preliminary nature, and the structure of the absorbing species has not been identified.

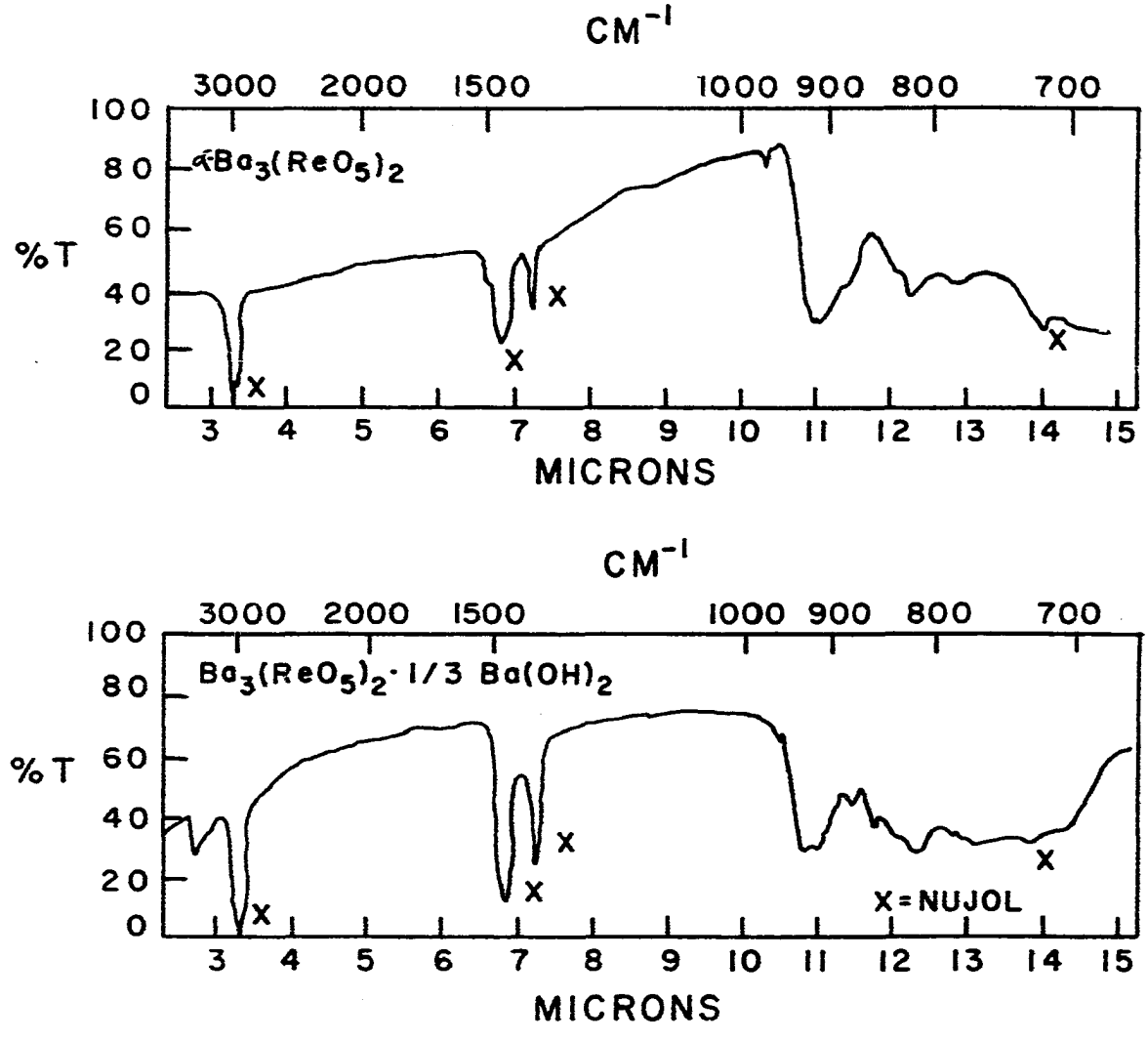

Figure 15. Near infrared spectra (in Nujol) of α-$Ba_3(ReO_5)_2$ (top) and $Ba_3(ReO_5)_2 \cdot 1/3\ Ba(OH)_2$ (bottom)

and 823 cm^{-1}. The $Ba_3(ReO_5)_2 \cdot 1/3\ Ba(OH)_2$ spectrum shows the hydroxyl stretching mode at 3593 cm^{-1} and other absorptions at 953 cm^{-1} (a shoulder), 937 cm^{-1}, 858 cm^{-1}, and 817 cm^{-1}.

It is well established that metal-oxygen stretching frequencies occur in the range of 900-1100 cm^{-1} (97), therefore, the positions of mesoperrhenate absorptions are not unexpected. (ReO_4^-, ReO_3Cl, ReO_3Br, and Re_2O_7 also show absorption in this range (98).) The assignment of particular absorption bands to the mesoperrhenate normal modes of vibration is not straight forward, however. If crystal effects are small, C_{4v} symmetry can be assumed to apply to the ion in its crystal environment, but distortions from ideal geometry could lead to spectral broadening. A normal coordinate analysis for C_{4v} symmetry has been calculated by Stephenson and Jones (99). The analysis shows three infrared active stretching modes of vibration: $A_1 + A_1 + E$. For ReO_5^{-3}, the A_1 modes describe the stretching of the rhenium-oxygen bonds: one mode is the rhenium and apex oxygen stretch and the other the stretching between rhenium and the basal oxygens. In view of the short $Re\text{-}O_3$ bond distance, it seems reasonable to assign the stretching of this bond to the bands of highest oscillator

strength, the 975 cm^{-1} peak in the α-$Ba_3(ReO_5)_2$ spectrum and the 953 cm^{-1} absorption in the $Ba_3(ReO_5)_2 \cdot 1/3\ Ba(OH)_2$ spectrum.

BIBLIOGRAPHY

1. Cherdyntsev, V. V., Abundance of Chemical Elements. Chicago, Ill., The University of Chicago Press. c1961.

2. Churchward, P. E. and Rosenbaum, J. B., U.S. Bureau of Mines Report of Investigations RI-6246. 1963.

3. Spelman, J. W., Metal Progr. 93, 103 (1968).

4. Mendeleeff, D. I., J. Chem. Soc. 55, 634 (1889).

5. Lebedev, K. B., Rhenium, Translated by U.S. Department of Commerce, Office of Technical Services, Joint Publications Research Service JPRS-23,361. 1964.

6. Druce, J. G. F., Rhenium. Great Britain, Cambridge University Press. 1948.

7. Noddack, W., Tacke, I., and Berg, O., Naturwissenschaften 13, 567 (1925).

8. Noddack, I. and Noddack, W., Z. Anorg. u. Allgem. Chem. 183, 353 (1929).

9. Noddack, I. and Noddack, W., Z. Physik. Chem. (Leipzig) A. 154, 207 (1931).

10. Fleischer, M., Econ. Geol. 54, 1406 (1959).

11. Malouf, E. E. and Zimmerley, S. R., Mineralogical and Geological Occurrence of Rhenium. In Gonser, B. W., ed. Rhenium. Pp. 3-5. Amsterdam, Netherlands, Elsevier Publishing Company. 1962.

12. Kosyak, E. A., Vestn. Akad. Nauk Kaz. SSR 21, 52 (1965). In Russian. Original not available; abstracted in Chemical Abstracts 63: 16037e. 1965.

13. Satpaev, K. I., Geokhimiya 1965, 1004 (1965). In Russian. Original not available; abstracted in Chemical Abstracts 63: 16037h. 1965.

14. McInnis, W., Molybdenum, U.S. Bureau of Mines Bulletin 585. 1960.

15. Feit, W., Z. Angew. Chem. 43, 459 (1930).

16. Feit, W., Angew. Chem. 46, 216 (1933).

17. Melaven, A. D., Rhenium. In Hampel, C. A., ed. Rare Metals Handbook. 2nd ed. Pp. 418-433. New York, New York, Reinhold Publishing Corp. c1961.

18. Davenport, W. H., Chem. Eng. 70(6), 86 (1963).

19. Malouf, E. E., Prater, J. D., and Zimmerley, S. R., Metallurgical Processes for Recovery of Rhenium from Flue Dusts and Gases. In Gonser, B. W., ed. Rhenium. Pp. 6-12. Amsterdam, Netherlands, Elsevier Publishing Company. 1962.

20. Wilhelm, H. A., U.S. Atomic Energy Commission Report IS-2029 (Iowa State University of Science and Technology, Ames Institute for Atomic Research). 1967.

21. Melaven, A. D., Rhenium. In Hampel, C. A., ed. Rare Metals Handbook. Pp. 347-364. New York, New York, Reinhold Publishing Corp. c1954.

22. Port, J. H., Rhenium and Rhenium Alloy Technology, Technical paper presented at the Annual Meeting of the American Institute of Mining, Metallurgical and Petroleum Engineers, New York, New York, February 16-24, 1964. Waterbury, Connecticut, Chase Brass and Copper Co. 1964.

23. Jungfleisch, M. and Ruff, H., Process for the Production of Pure Rhenium and Its Compounds. In Gonser, B. W., ed. Rhenium. Pp. 13-19. Amsterdam, Netherlands, Elsevier Publishing Company. 1962.

24. Davenport, W. H., Rhenium Sources and Methods of Extraction and Refining, Technical Paper presented at the Annual Meeting of the American Institute of Mining, Metallurgical, and Petroleum Engineers, New York, New York, February 16-24, 1964. Waterbury, Connecticut, Chase Brass and Copper Co. 1964.

25. Davenport, W. H., Kollonitsch, V., and Kline, C. H., Ind. Eng. Chem. 60, 10 (1968).

26. Traill, R. J., Can. Mineralogist 7, 524 (1963).

27. Dickinson, R. G. and Pauling, L., J. Amer. Chem. Soc. 45, 1466 (1923).

28. Jellinek, F., Braüer, G., and Müller, H., Nature (London) 185, 376 (1960).

29. Swanson, H. E., Gilfrich, N. T., and Ugrinic, G. M., U.S. National Bureau of Standards Circular 539(V). 1955.

30. Bell, R. E. and Herfert, R. E., J. Amer. Chem. Soc. 79, 3351 (1957).

31. Lagrenaudie, J., J. Phys. Radium 15, 299 (1954).

32. Jellinek, F., Arkiv Kemi 20, 447 (1963).

33. Kagle, (initials unknown), unpublished paper cited in Malouf, E. E. and Zimmerley, S. R., Mineralogical and Geological Occurrence of Rhenium. In Gonser, B. W., ed. Rhenium. Pp. 3-5. Amsterdam, Netherlands, Elsevier Publishing Company. 1962.

34. Palino, G. F., Neutron Activation Analysis of Rhenium in Rocks. Unpublished M.S. thesis. Ames, Iowa, Library, Iowa State University of Science and Technology. 1965.

35. Roman, R. J., Bhappu, R. B., and Reynolds, D. H., Trans. Met. Soc. AIME. 233, 2051 (1965).

36. Yusupova, A. B. and Songina, O. A., Izv. Akad. Nauk Kaz. SSR, Ser. Khim. Nauk 15, 15 (1965). Original not available; abstracted in Chemical Abstracts 64: 7738c. 1966.

37. Bhappu, R. B., Reynolds, D. H. and Stahmann, W. S., New Mexico State Bureau of Mines and Mineral Resources Circular 66. 1963.

38. Bhappu, R. B., Reynolds, D. H. and Roman, R. J., J. Metals 17, 1199 (1965).

39. Schäfer, H., Chemical Transport Reactions. New York, New York, Academic Press Inc. c1964.

40. Nitsche, R., Bölsterli, H. U. and Lichtensteiger, M., J. Phys. Chem. Solids 21, 199 (1961).

41. Glukhov, I. A., Davidyants, S. B., Yunusov, M. A. and El'manova, N. A., J. Inorg. Chem. USSR 6 (6), 649 (1961).

42. Traore, K., Bull. Soc. Chim. France, 1284 (1965).

43. Magneli, A., Acta Chem. Scand. 11, 28 (1957).

44. Meisel, K., Z. Anorg. Chem. 207, 121 (1932).

45. Ferretti, A., Rogers, D. B., and Goodenough, J. B., J. Phys. Chem. Solids 26, 2007 (1965).

46. Sims, C. T., Properties of Rhenium. In Gonser, B. W., ed. Rhenium. Pp. 23-35. Amsterdam, Netherlands, Elsevier Publishing Company. 1962.

47. Krebs, B., Müller, A., and Beyer, H. Chem. Comm., 263 (1968).

48. Smith, W. T., Line, L. E., and Bell, W. A., J. Amer. Chem. Soc. 74, 4964 (1952).

49. Noddack, I. and Noddack, W., Naturwissenschaften 17, 93 (1929).

50. Noddack, I. and Noddack, W., Z. Anorg. u. Allgem. Chem. 181, 1 (1929).

51. Noddack, I. and Noddack, W., Das Rhenium. Germany, Voss. 1933.

52. Ogawa, E., J. Chem. Soc. Japan 7, 265 (1932).

53. Briscoe, H. V. A., Robinson, P. L., and Rudge, A. J., J. Chem. Soc., 1104 (1932).

54. Hagen, H. and Sieverts, A., Z. Anorg. u. Allgem. Chem. 208, 367 (1932).

55. Tribalat, S., Rhenium et Technetium. Paris, Gauthier-Villars. 1957.

56. Woolf, A. A., Quart. Rev. (London) 15, 372 (1961).

57. Peacock, R. D., The Chemistry of Technetium and Rhenium. Amsterdam, Netherlands, Elsevier Publishing Co. 1966.

58. Colton, R., The Chemistry of Rhenium and Technetium. Great Britain, Interscience Publishers. 1965.

59. Sargent, J. D., Rhenium. U.S. Bureau of Mines Bulletin 556. 1956.

60. Lebedev, K. B. The Chemistry of Rhenium. London, Butterworths and Co. 1962.

61. Melaven, A. D., Fowle, J. N., Bricknell, W., and Hiskey, C. F., Inorganic Synthesis III, 188 (1950).

62. Willard, H. H. and Smith, G. M., Anal. Chem. 11, 305 (1938).

63. Berry, K. O., Condensed Phase and Vaporization Equilibria in Vanadium(II) Halide-Iodine Systems. Unpublished Ph.D. thesis. Ames, Iowa, Library, Iowa State University of Science and Technology. 1966.

64. Gibbs, W. E., Clouds and Smokes. London, J. and A. Churchill. 1924.

65. Green, H. L. and Lane, W. R., Particulate Clouds: Dusts, Smokes and Mists. London, E. and F. N. Spon Ltd. 1957.

66. Remy, H., Treatise on Inorganic Chemistry. Vol. II. Netherlands, Elsevier Publishing Company. 1956.

67. Walmsley, H. P., Phil. Mag. 7, 1097 (1929).

68. Turkevich, J., Ultrafine Particles in the Gas Phase. In Bonis, L. J., de Bruyn, P. L., and Duga, J. J. eds. Fundamental Phenomena in the Materials Sciences III. Pp. 195-212. New York, N.Y., Plenum Press. 1966.

69. Noddack, I. and Noddack, W., Z. Anorg. u. Allgem. Chem. 215, 129 (1933).

70. Scharnow, B., Z. Anorg. u. Allgem. Chem. 215, 185 (1933).

71. Scholder, R., Angew. Chem. 70, 583 (1958).

72. Scholder, R., Huppert, K. L., and Pfeiffer, P. P., Angew. Chem. 75, 375 (1963).

73. Scholder, R. and Huppert, K. L., Z. Anorg. u. Allgem. Chem. 334, 209 (1964).

74. Carrington, A. and Symons, M. C. R., J. Chem. Soc., 284 (1960).

75. Sleight, A. W. and Ward, R., J. Amer. Chem. Soc. 83, 1088 (1961).

76. Williams, D. E., U.S. Atomic Energy Commission Report IS-1052 (Iowa State University of Science and Technology, Ames Institute for Atomic Research). 1964.

77. Alexander, L. E. and Smith, G. S., Acta Cryst. 15, 983 (1962).

78. Busing, W. R. and Levy, H. A., Acta Cryst. 10, 180 (1957).

79. Benson, J. E., The Crystal Structure of Sodium Hydrogen Fluoride. Unpublished M.S. thesis. Ames, Iowa, Library, Iowa State University of Science and Technology. 1963.

80. Williams, D. E. and Rundle, R. E., J. Amer. Chem. Soc. 86, 1660 (1964).

81. Henry, N. F. M. and Lonsdale, K., eds., International Tables for X-Ray Crystallography. Vol. I. Birmingham, England, The Kynoch Press. 1952.

82. Busing, W. R., Martin, K. O., and Levy, H. A., U.S. Atomic Energy Commission Report ORNL-TM-305 (Oak Ridge National Laboratory, Tenn.). 1962.

83. Hanson, H. P., Herman, F., Lea, J. D., and Skillman, S., Acta Cryst. 17, 1040 (1964).

84. Lonsdale, K., ed., International Tables for X-Ray Crystallography. Vol. III. Birmingham, England, The Kynock Press. 1962.

85. Hamilton, W. C., Acta Cryst. 18, 502 (1965).

86. Johnson, C. K., U.S. Atomic Energy Commission Report ORNL-3794 (Oak Ridge National Laboratory, Tenn.). 1965.

87. Hamilton, W. C., Acta Cryst. 12, 609 (1959).

88. Busing, W. R., Martin, K. O., and Levy, H. A., U.S. Atomic Energy Commission Report ORNL-TM-306 (Oak Ridge National Laboratory, Tenn.). 1964.

89. Slater, J. C., Quantum Theory of Molecules and Solids. Vol. 2. New York, New York, McGraw-Hill, Inc. 1965.

90. Pauling, L., The Nature of the Chemical Bond. Ithaca, New York, Cornell University Press. 1960.

91. Lipson, H. and Cochran, W., The Determination of Crystal Structures. Ithaca, New York, Cornell University Press. 1966.

92. Stout, G. H. and Jensen, L. H., X-Ray Structure Determination. New York, New York, The Macmillan Company. 1968.

93. Gillespie, R. J., J. Chem. Soc., 4672 (1963).

94. Amble, E., Miller, S. L., Schawlaw, A. L., and Townes, C. H., J. Chem. Phys. 20, 192 (1952).

95. Morrow, J. C., Acta Cryst. 13, 443 (1960).

96. Rulfs, C. L., U.S. Atomic Energy Commission Report COO-1483-2 (Chicago Operations Office, AEC). 1968. (Distribution of this document is limited to Government Agencies and their contractors).

97. Barraclough, C. G., Lewis, J., and Nyholm, R. S., J. Chem. Soc., 3552 (1959).

98. Nakamoto, K., Infrared Spectra of Inorganic and Coordination Compounds. New York, New York, John Wiley and Sons, Inc. 1963.

99. Stephenson, C. V. and Jones, E. A., J. Chem. Phys. 20, 1830 (1952).

100. Birks, L. S. and Friedman, H., J. App. Phys. 17, 687 (1946).

ACKNOWLEDGEMENT

The author thanks Dr. Harley A. Wilhelm for his assistance during the course of this research. Dr. Wilhelm has allowed the author considerable freedom in the choice of the research problems and in pursuing their solutions, and the experiences gained from these latitudes are gratefully acknowledged.

APPENDICES

Appendix A. A Crystallite Size Calculation for the White Rhenium Oxide

Superimposed densitometer tracings of the X-ray diffraction photographs for white and yellow rhenium oxides have been illustrated in Figure 8 of the text. The diffraction band of the white oxide is centered at 25.16° in two theta. The 211, 040, and 221 diffraction peaks of Re_2O_7 (the three most intense lines of the entire pattern) are centered at 22.35°, 23.34°, and 24.54° respectively. For the purposes of this crystallite size calculation, the white oxide diffraction band is assumed to arise from three broadened diffraction peaks resulting from the 211, 040, and 221 reflections of Re_2O_7.

Line broadening is related to crystallite size by the following equation (100)

$$D = \frac{K\lambda}{B \cos \theta_{hk\ell}} \quad . \qquad (7)$$

D is the calculated mean diameter of the crystallite. λ = 1.54178Å. $\theta_{hk\ell}$ = 12.58° is the observed Bragg angle for the diffraction band. K is a shape constant taken here as 1.1 (100). B is the corrected peak broadening (in radians) which is derived from the equation (100)

$$B^2 = B'^2 - b'^2 .$$

B' is the measured width of the crystallite broadened peak at half of the maximum peak height. b' is an instrument constant equal to the width at half maximum of the diffraction peak for crystals greater than 1000Å. B was not corrected for α_1-α_2 broadening which is small at $\theta_{hk\ell} = 12.58^{\circ}$. B was also not corrected for strain broadening even though broadening can be induced in crystalline Re_2O_7[1]. The extent of strain broadening could not be estimated since only one diffraction band was observed, furthermore, the position of the band was shifted toward a greater Bragg angle which would imply a compressive straining force. Since compressive strain seems unlikely, the omission of a strain correction would appear justified. The shift to a greater diffraction angle possibly results from smaller lattice spacings brought about by reducing the number of distant neighboring atoms as the crystallite sizes become small. For an ionic lattice this would be analogous to termination of the Madelung constant series short of infinity.

---

[1]The half maximum widths of the diffraction peaks for the 211, 040, and 221 reflections of crystalline Re_2O_7 were broadened by about 35-40 percent upon grinding by hand in an agate mortar and pestle. The broadening was symmetric about $\theta_{hk\ell}$ and disappeared after annealing for 24 hours at 50°C.

b' was determined as .0483 radians (the angle between the 211 and 221 diffraction peaks) and B' was determined from the broadened band as .102 radians. The calculated average diameter of the crystallites, according to Equation 7, is about 20Å. Since this calculated crystallite size was determined from a large estimated instrument constant, the calculated value should only be interpreted as an indication of magnitude.

Appendix B. An α-$Ba_3(ReO_5)_2$ Powder Diffraction Study

With the aid of Weissenberg and precession X-ray diffraction photographs, the reflections of α-$Ba_3(ReO_5)_2$ were indexed in the hexagonal crystal system (apparent Laue symmetry 6/mmm). The lattice constants and their estimated standard deviations were obtained from a least-squares refinement (76) of 24 independent reflection angles observed for powder samples at room temperature with a Norelco diffractometer equipped with a proportional counter and a strip chart recorder. A flat plate specimen geometry was used with copper Kα radiation ($\lambda_{K\alpha}$ = 1.54178Å). No extrapolation function was employed during the least-squares refinement because the reflection angles were small. The determined unit cell parameters and their estimated standard deviations are a = 10.726 $\pm$ .003Å and c = 8.246 $\pm$ .004Å.

A listing of the observed diffraction angles (two theta), the calculated diffraction angles, and the relative intensities is given in Table 10. The relative intensities were obtained by weighing paper cut-outs of the tracings from the strip chart recordings of the diffraction peaks.

Table 10. X-ray powder data for α-$Ba_3(ReO_5)_2$

Reflection (hkℓ)	Diffraction angle (two theta) observed	calculated[a]	Relative intensity
110	16.50	16.53	5
200	19.15	19.11	3
111	19.80	19.75	13
002	21.60	21.55	17
210	25.40	25.37	10
112	27.30	27.28	100
211	27.62	27.61	79
300	28.85	28.83	80
221	35.20	35.19	3
302	36.10	36.28	6
311	36.55	36.54	32
400	38.80	38.78	3
222	40.12	40.11	33
213	41.74	41.73	17
321	43.90	43.88	--
004	43.90	43.92	--
500	49.00	49.03	4
412	50.12	50.15	13
330	51.05	51.09	3
420	52.05	52.10	5
331	52.30	52.37	4
502	54.12	54.15	13
422	57.00	57.02	6
522	66.85	66.87	7

[a] $a = 10.726\text{Å}$, $c = 8.246\text{Å}$, $\lambda = 1.54178\text{Å}$.

Appendix C. A Listing of Crystallographic Equations

Presented below are the functional forms of some of the equations used for the treatment of X-ray intensity data and for the solution of the $Ba_3(ReO_5)_2 \cdot 1/3\ Ba(OH)_2$ crystal structure.

Streak intensity equations

$$I_{stk} = \sum_{n>m\geq n/2} \frac{\cos \theta_n}{\sin \theta_n} K(\lambda m)\ I_m$$

I_{stk} is the streak contribution to the measured intensity of reflection nh, nk, nℓ where n is an integer.

I_m is the integrated intensity of reflection mh, mk, mℓ where m<n. I_m is corrected for Lorentz-polarization effects.

$K(\lambda m)$ is a streak constant obtained experimentally from the measurement of the 502, 304, 421, and 115 reflections.

θ_n is the Bragg angle for reflection nh, nk, nℓ.

$$\sigma(I_{stk})^2 = \left(\frac{\partial I_{stk}}{\partial K(\lambda m)}\right)^2 \sigma^2(K(\lambda m)) + \left(\frac{\partial I_{stk}}{\partial I_m}\right)^2 \sigma^2(I_m)$$

$\sigma^2(I_m)$ is the variance of I_m which was defined in the text.

$\sigma^2(K(\lambda_m))$ is the variance of the streak constant which was assigned as $(0.05\ K(\lambda_m))^2$.

Patterson function (general)

$$P(u,v,w) = V \iiint \rho(x,y,z)\ \ \rho(x+u,y+v,z+w)\ \ dx\ dy\ dz$$

$$P(u,v,w) = \frac{1}{V} \sum_{h} \sum_{k=-\infty}^{\infty} \sum_{\ell} |F_{hk\ell}|^2 \cos 2\pi(hu + kv + \ell w)$$

V is the volume of the unit cell.

$\rho(x,y,z)$ is the electron density at the fractional coordinates x, y, z of the unit cell.

h, k, ℓ are the Miller indices of the lattice planes.

Patterson function (hexagonal crystal system) (81)

$$P(u,v,w) = \frac{4}{V} \sum_{h} \sum_{k=o}^{\infty} \sum_{\ell} \left(|F_{hk\ell}|^2 \cos 2\pi(hu+kv) + |F_{\bar{h}k\ell}|^2 \cos 2\pi(hu-kv) \right) \cos 2\pi \ell w$$

Structure factor equations

$$F_{hk\ell} = \sum_{n=1}^{N} f_n \, e^{2\pi i(hx+ky+\ell z)} \, e^{-T_n} \equiv A_{hk\ell} + i\, B_{hk\ell}$$

$$|F_{hk\ell}| = \sqrt{A_{hk\ell}^2 + B_{hk\ell}^2}$$

$$A_{hk\ell} = \sum_{n=1}^{N} f_n \cos 2\pi(hx+ky+\ell z) \, e^{-T_n}$$

$$B_{hk\ell} = \sum_{n=1}^{N} f_n \sin 2\pi(hx+ky+\ell z) \, e^{-T_n}$$

$$\alpha_{hk\ell} = \tan^{-1} \left(\frac{B_{hk\ell}}{A_{hk\ell}} \right)$$

n is an index used for summation over the N atoms in the unit cell.

f_n is the atom scattering factor for the nth atom.

T_n is the appropriate temperature factor for the nth atom. (isotropic or anisotropic)

$\alpha_{hk\ell}$ is the phase angle of the diffracted wave.

Electron density Fourier synthesis

$$\rho(x,y,z) = \frac{1}{V} \sum_h \sum_k \sum_\ell F_{hk\ell}\, e^{-2\pi i(hx+ky+\ell z)}$$

$$= \frac{1}{V} \sum_h \sum_k \sum_\ell |F_{hk\ell}| e^{2\pi i\alpha_{hk\ell}}\, e^{-2\pi i(hx+ky+\ell z)}$$

Electron density difference Fourier synthesis

$$\rho(x,y,z)_{observed} - \rho(x,y,z)_{calculated} =$$

$$\frac{1}{V} \sum_h \sum_k \sum_\ell (|F_{hk\ell}|_o - |F_{hk\ell}|_c)\, e^{2\pi i\alpha_{hk\ell}}\, e^{-2\pi i(hx+ky+\ell z)}$$

Electron density difference Fourier synthesis for space group No. 185 (81)

$$\Delta\rho(x,y,z) = \frac{4}{V}\left\{\sum_h \sum_{\substack{k \\ o}}^{\infty} \sum_{\ell=2n} \left((|F_{hk\ell}|_o - |F_{hk\ell}|_c)\cos 2\pi(hx+ky)\right.\right.$$

$$\cos(2\pi\ell z - \alpha_{hk\ell}) + (|F_{\bar{h}k\ell}|_o - |F_{\bar{h}k\ell}|_c)\cos 2\pi(hx-ky)$$

$$\cos(2\pi \ell z - \alpha_{\bar{h}k\ell})\Big) \; - \sum_{h} \sum_{\substack{k \\ 0}}^{\infty} \sum_{\ell=2n+1} \Big(\big(|F_{hk\ell}|_o - |F_{hk\ell}|_c\big)$$

$$\sin 2\pi(hx+ky) \sin(2\pi \ell z - \alpha_{hk\ell}) -$$

$$\big(|F_{\bar{h}k\ell}|_o - |F_{\bar{h}k\ell}|_c\big) \sin 2\pi(hx-ky) \sin(2\pi \ell z - \alpha_{\bar{h}k\ell})\Big)\Big\} \quad .$$